AIAA

AIAA 2000-2602

A Sample of NASA Langley Unsteady Pressure Experiments for Computational Aerodynamics Code Evaluation

David M. Schuster, Robert C. Scott, Robert E. Bartels, John W. Edwards, and Robert M. Bennett
NASA Langley Research Center, Hampton, VA 23681

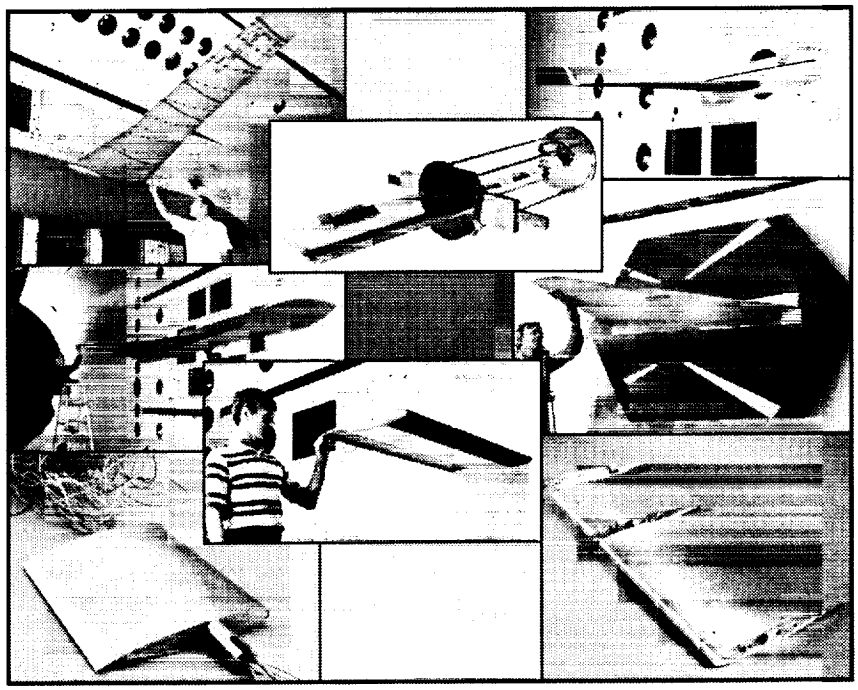

Fluids 2000 Conference and Exhibit
June 19–22, 2000/Denver, CO

A Sample of NASA Langley Unsteady Pressure Experiments for Computational Aerodynamics Code Evaluation

David M. Schuster,* Robert C. Scott,† Robert E. Bartels,‡ John W. Edwards,§ and Robert M. Bennett¶
NASA Langley Research Center, Hampton, VA 23681

As computational fluid dynamics methods mature, code development is rapidly transitioning from prediction of steady flowfields to unsteady flows. This change in emphasis offers a number of new challenges to the research community, not the least of which is obtaining detailed, accurate unsteady experimental data with which to evaluate new methods. Researchers at NASA Langley Research Center (LaRC) have been actively measuring unsteady pressure distributions for nearly 40 years. Over the last 20 years, these measurements have focused on developing high-quality datasets for use in code evaluation. This paper provides a sample of unsteady pressure measurements obtained by LaRC and available for government, university, and industry researchers to evaluate new and existing unsteady aerodynamic analysis methods. A number of cases are highlighted and discussed with attention focused on the unique character of the individual datasets and their perceived usefulness for code evaluation. Ongoing LaRC research in this area is also presented.

Introduction

COMPUTATIONAL Fluid Dynamics (CFD) methods are rapidly maturing and are being heavily integrated into the day-to-day design and analysis of modern aerospace systems. Even though most modern CFD codes are written in a time-accurate formulation, the cost of unsteady simulations has been exorbitant, and the majority of development and application has focused on prediction of steady flows. In addition, the design and analysis demands for CFD have historically been for steady flow problems, and the applications of the codes for unsteady problems have essentially been relegated to a research exercise. However, as computer systems continue to evolve, unsteady simulations are becoming increasingly practical. Design engineers are also in need of more refined information on phenomena such as buffet onset, flutter, potential limit cycle oscillations (LCO), and other nonlinear dynamic phenomena that can have a severe impact on a given system's performance. Thus, there is an increasing requirement for new algorithms and methodologies capable of accurately and efficiently predicting nonlinear unsteady flows. Detailed experiments highlighting various unsteady flow phenomena will also be required to assist researchers in evaluating, validating and guiding development of these methods. As the numerical methods and strategies required to predict unsteady flows are complex and labor intensive, thus are the experiments supporting these methods. Static pressure measurements have been the mainstay for steady code validation and evaluation, and unsteady pressure measurements will likewise be the primary source of data for the development of unsteady methods.

Researchers at NASA Langley Research Center (LaRC) have been acquiring unsteady pressure data for nearly 40 years. These measurements have addressed buffet, flutter, rigid body motion, and control system actuation, and numerous nonlinear unsteady aerodynamic and aeroelastic interactions. A comprehensive history of unsteady pressure measurements in the LaRC Transonic Dynamics Tunnel (TDT) is provided in reference 1. The present paper provides a more detailed discussion of a subset of these tests with an additional test case that was not presented in the overview paper.

For the past 20 years, LaRC researchers have been acquiring detailed unsteady pressure data specifically for the purpose of unsteady aerodynamic and aeroelastic code evaluation. Eleven of these cases are presented in this paper ranging in complexity from a simple two-dimensional airfoil tested under static and forced pitch oscillation conditions to more complex three dimensional wings undergoing forced rigid-body oscillations

*Research Engineer, Aeroelasticity Branch, Structures and Materials, Associate Fellow, AIAA.
†Research Engineer, Aeroelasticity Branch, Structures and Materials, Senior Member, AIAA.
‡Research Engineer, Aeroelasticity Branch, Structures and Materials, Senior Member, AIAA.
§Research Engineer, Aeroelasticity Branch, Structures and Materials, Associate Fellow, AIAA.
¶Research Engineer, Aeroelasticity Branch, Structures and Materials, Associate Fellow, AIAA.

Table 1 Wind-Tunnel Test Programs.

Wind-Tunnel Test Program	Data Types
High Re Supercritical Airfoil	Rigid Airfoil, Pitch Oscillations
Rectangular Supercritical Wing	Rigid Wing, Pitch Oscillations
Clipped Delta Wing	Rigid Wing, Pitch Oscillations, Trailing Edge Control Surface Surface
BMP - B0012	Rigid Wing, Flutter on PAPA
BMP - B64A010	Rigid Wing, Flutter on PAPA
BMP - BSCW	Rigid Wing, Flutter on PAPA
BACT	Rigid Wing, Flutter on PAPA, Active Spoilers and Aileron
DAST ARW-2 Wing	Flexible Wing, Trailing Edge Control Surface
HSR - RSM	Rigid Wing, Trailing Edge Control Surface, Flutter on PAPA
HSR - FSM	Flexible Wing, Trailing Edge Control Surface, Flutter
MAVRIC I	Flexible Wing, Flutter/LCO

to highly complex structurally flexible geometries. A list of these cases, and their general characteristics are presented in table 1. Each of these cases will be described and discussed in detail focusing on the characteristics of each dataset that make it unique and valuable for code validation. Supporting data, such as geometric and structural characteristics, are presented for each case. When available, computations performed using data resulting from these tests will be presented and/or cited by reference.

Test Facilities

A high-Reynolds number supercritical airfoil test was conducted in the LaRC 0.3-Meter Transonic Cryogenic Tunnel (0.3m TCT). At the time of the test, this tunnel had a rectangular cross section that was eight inches wide with slotted floor and ceiling. The test medium for this tunnel is nitrogen, and it serves as a pilot tunnel for LaRC's National Transonic Facility. This test was conducted at Reynolds numbers ranging from 12 to 70 million per foot. These high Reynolds number conditions make this test case an especially unique dataset for code validation.

All of the remaining tests were conducted in the TDT.[2] The TDT is a closed circuit, continuous-flow wind tunnel capable of testing at stagnation pressures from near zero to atmospheric conditions and over a Mach number range from zero to 1.2. The test section of the TDT is 16 feet square with cropped corners. Controlled variation of pressure in the tunnel simulates variations in flight altitude. Tests can be performed in the TDT using air as the test medium, however, the most distinguishing feature of the tunnel is the use of a heavy gas, presently R-134a refrigerant. R-134a is about four times as dense as air, yet has a speed of sound of about half that of air. These properties of higher density and lower sonic speed have beneficial effects on the design, fabrication, and testing of aeroelastically scaled wind-tunnel models. Other advantages resulting from the use of a heavy gas are a nearly three-fold increase in Reynolds number and lower tunnel drive horsepower compared to those for air. Note that prior to 1997 the heavy gas used in the TDT was R-12, and many of the aerodynamic data sets described in this paper were obtained in R-12. A recent series of papers[1-6] provide a complete overview and history of the TDT.

Comments on Test Case Selection and Presentation Order

The eleven test cases are presented in order of increasing modeling complexity. The prospective user of these data may begin with the first case that involves modeling only a rigid two-dimensional airfoil with no control surfaces, and gradually progress through more complex configurations and computational challenges to cases involving three-dimensional geometries, structural flexibility, and controls. In reality, the flow conditions at which the individual cases were tested may make the seemingly simpler cases more of a computational challenge than some of the perceived more complex cases. Each of these datasets presents a unique set of flowfield physics and computational challenges. It is precisely this wide variety of features that make this collection an outstanding resource for unsteady CFD evaluation and validation.

High Reynolds Number Supercritical Airfoil

The advent of cryogenic wind tunnels provided the capability to simulate flight Reynolds Numbers with reasonably sized models and relatively low dynamic pressures. This section reviews an unsteady pressure test of an oscillating airfoil in NASA Langley's 0.3-Meter Transonic Cryogenic Tunnel. A discussion of the test program and an overview of results is given by Hess et al.[7]

Physical Description

The model, shown in figure 1, was an SC(2)-0714 supercritical airfoil with 14 percent thickness to chord ratio. It had a 6 inch chord, an 8 inch span, and was oscillated hydraulically about a 35 percent chord pitch axis. Forty-three unsteady pressure transducers

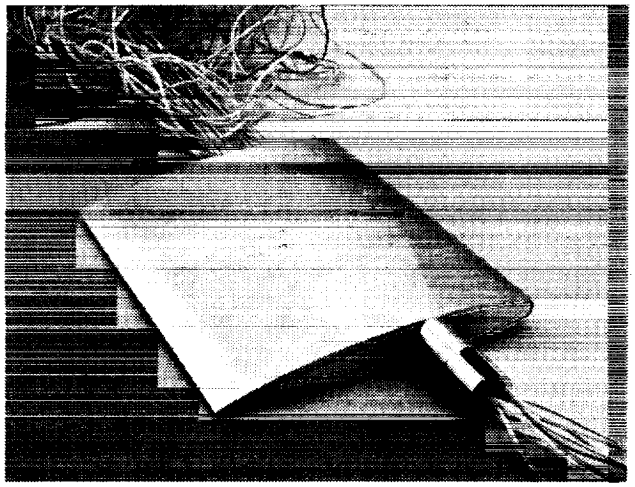

Fig. 1 High Reynolds Number Supercritical Wing.

were mounted internally in rows near the midspan. The transducer layout is given in reference 7. A novel plumbing arrangement was employed for the reference pressures for the unsteady pressure transducers which involved shortened tube lengths from reference orifices and flow restrictors to provide steady, mean reference pressures.

Experimental Data

Three forms of pressure data were taken during the test; steady, unsteady due to airfoil oscillations, and unsteady with no airfoil oscillation (shock buffet data, called "turbulence" data in reference 7). Steady data was acquired on the tunnel's analog data acquisition system utilizing low pass filters and averaging. Unsteady data was acquired on two 28 channel analog tape recorders. The airfoil oscillation data was analyzed following the test by digitizing the data at 32 samples per cycle for 64 cycles and performing Fast Fourier Transform analysis to extract the first 3 fundamental harmonics of the oscillation frequency. The raw turbulence data time histories were digitized at 5000 samples per second. Test conditions were: Mach numbers (M) of 0.65, 0.70, 0.72, and 0.74 and Reynolds numbers from 6 to 35 million based on chord. The most complete data were taken at M=0.72 and Re=15 and 30 million. The mean angle of attack was varied from -2.5 to +3.0 degrees in 0.5 degree increments. The airfoil was oscillated at frequencies of 5, 20, 40, and 60 Hz. and at amplitudes of 0.25, 0.50, and 1.00 degree. Figure 2 is a sample of steady pressure data showing the effect of Reynolds number on shock location for M = 0.72 and 2.5 degrees angle of attack.

Following the test, a slight time misalignment from 0.001 to 0.040 seconds, was found between the data sets on the two recorders which has complicated time correlations for the oscillating airfoil cases. In contrast, the shock buffet data has been very useful since the test conditions encompassed several cases of buffet airloads caused by shock boundary-layer interaction

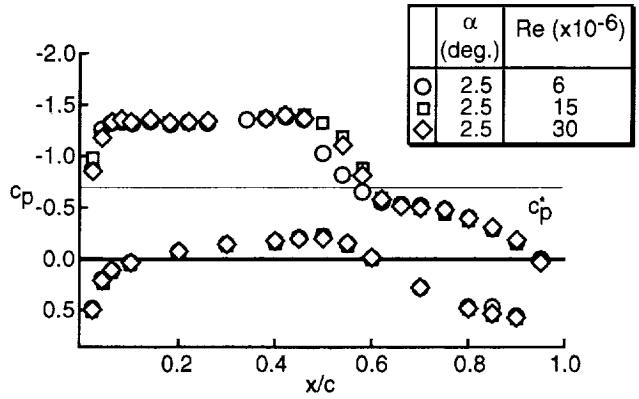

Fig. 2 Steady chordwise pressure coefficients for SC(2)-0714 airfoil, $M = 0.72$.

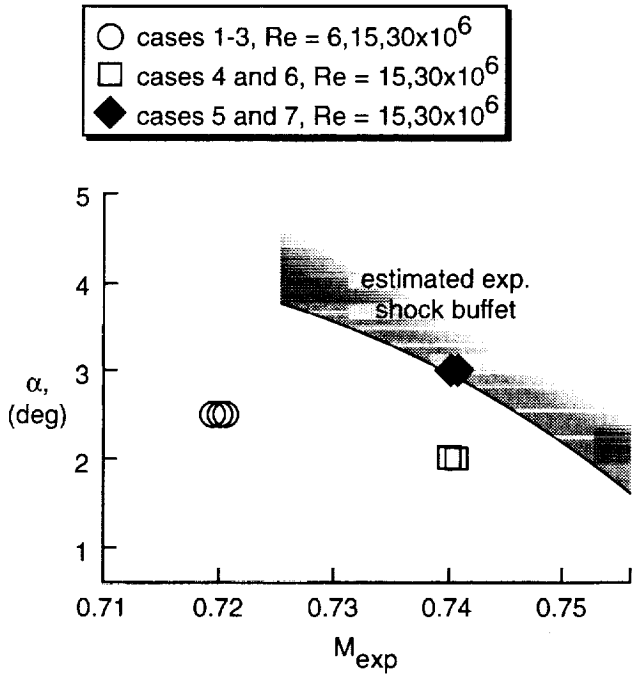

Fig. 3 Steady and shock buffet conditions for the SC(2)-0714 airfoil.

and separation. These cases are of significant interest for CFD code validation of capability for such challenging unsteady viscous interactions. Bartels and Edwards[8] discuss seven of the turbulence data cases, including two cases of "shock buffet" at M = 0.74 and 3.0 degrees angle of attack. These conditions are shown in figure 3. Power spectral densities of pressure distributions exhibit the self-excited shock oscillation characteristic of the transonic buffet conditions. The shock oscillations are very coherent with frequencies near 70 Hz. Reduced frequencies are in the range 0.19-0.21 at Reynolds number of 15 million and 0.20-0.23 at Reynolds number of 30 million.

Finally, a fourth data set was taken during this test by Ng and Rosson[9] who measured unsteady wake pressures with a dual hot-wire aspirating probe on a traversing rake assembly. Of most interest with regard

to unsteady airfoil pressure measurements are the frequency spectra observed in the settling chamber, the test section, and the wake probe. A strong frequency component is seen at the tunnel fan blade passage frequency in the settling chamber and from the wake probe as it approaches the wake centerline. Unpublished spectral data from the airfoil turbulence data cases also show strong frequency components at the fan blade passage frequency (700-900 Hz.) for conditions with regions of near-sonic flow over the airfoil.

Aerodynamic Models and Investigations

Bartels[10,11] has been successful in capturing the shock buffet cases computationally with an interactive boundary layer model and with a thin-layer Navier-Stokes code. The effect of Reynolds number scaling on the onset of shock buffet for this airfoil was investigated in the cited reports. Shock buffet onset can be defined as the transition from steady (incoherent low level unsteadiness) to shock induced oscillation driven by the interaction of the shock and separated boundary layer flow. In both experiment and computations the unsteady flow displays a well defined dominant fundamental frequency with minor higher harmonics. The fundamental frequency corresponds to the oscillation of the shock over a significant portion of the airfoil. Data samples from those reports showing the power spectral density of the pressure coefficient for the fundamental frequency are shown figures 4 and 5. Turbulent transition in the computations was at the leading edge; the variation with Reynolds number represents boundary layer Reynolds number scaling or thickness effects only. The shock buffet onset boundary shown in the computed data of figure 4 appears to match very closely the trend with Reynolds number shown in the experimental data of figure 5. Regarding the issue of validation of CFD codes for such viscous interaction at transonic conditions, attention is drawn to the problem of buffet onset for the NACA 0012 airfoil. An excellent unsteady pressure data set for this airfoil has been published by McDevitt and Okuno.[12] The shock oscillation conditions of the buffet onset boundary have been successfully calculated by Bartels[10,11] and Edwards[13] with interactive boundary layer models, whereas attempts to calculate this buffet onset boundary with a thin layer Navier-Stokes code[10,11] have been unsuccessful. This remains a challenging case for CFD methods.

Rectangular Supercritical Wing

In the early 1980's, a simple rectangular planform wing with a supercritical airfoil section was tested in the TDT to investigate the unsteady aerodynamic characteristics of wings employing supercritical airfoils, and to provide correlation data for CFD methods. This wing, known as the Rectangular Supercritical Wing (RSW),[14-16] was oscillated in pitch and

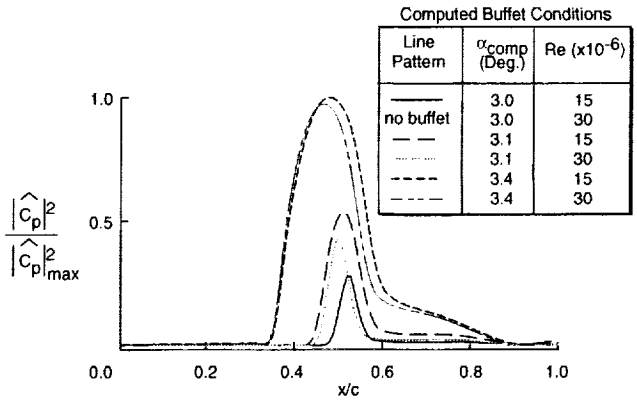

Fig. 4 Reynolds number scale effect on shock buffet (computed) for the SC(2)-0714 airfoil, M_{comp} = 0.725.

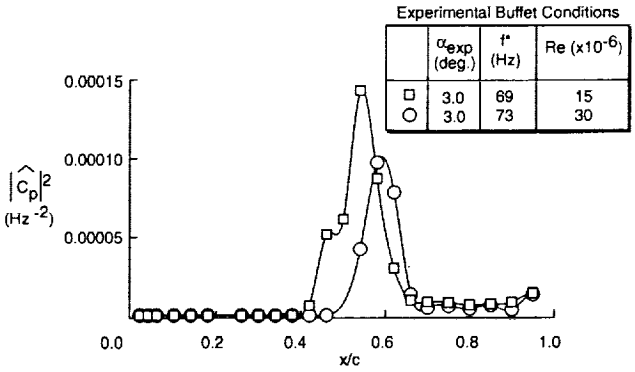

Fig. 5 Reynolds number scale effect on shock buffet (experiment) for the SC(2)-0714 airfoil, M = 0.74.

unsteady pressures were measured using a combination of in situ transducers and matched-tube orifices. A selection of computational test cases from this investigation are presented in references 17 and 18.

Physical Description

A photograph of the model installed in the TDT is shown in figure 6. The RSW had an unswept rectangular planform with a tip of revolution, a panel aspect ratio of 2.0, a twelve percent thick supercritical airfoil, and no twist. The constant airfoil section of the wing was 48 inches in span, and the tip of revolution made the overall span of the wing 49.43 inches. The wing chord was 24 inches. The airfoil for the RSW is shown in figure 7. It was derived from an 11 percent thick section[19] by increasing the thickness to 12 percent while maintaining the mean camber line. Reference 20 quotes the design Mach number and lift coefficient to be 0.80 and 0.60, respectively. A complete set of measured ordinates for the model are available, and in general, they compare very well with the theoretically derived airfoil contour.[17,18] The RSW was mounted to a splitter plate in the TDT to offset the model from the boundary layer formed along the wall of the wind tunnel. It was oscillated in pitch about the 46 percent

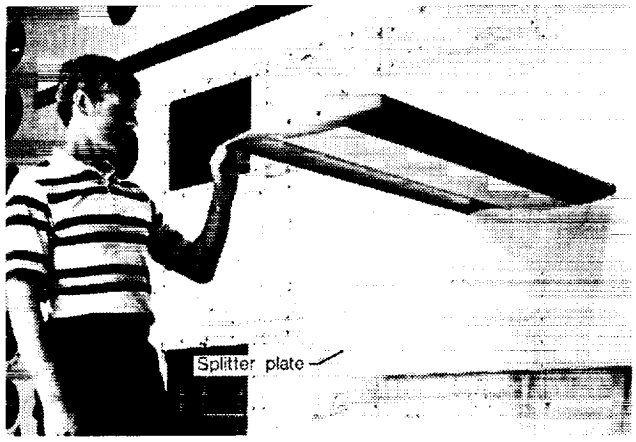

Fig. 6 Rectangular Supercritical Wing mounted on splitter plate in the TDT.

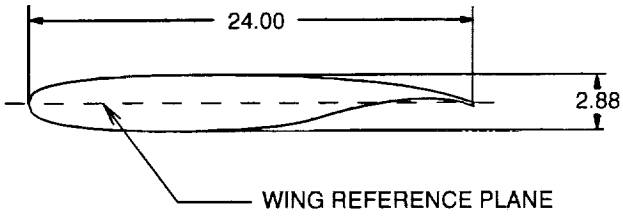

Fig. 7 Airfoil for the Rectangular Supercritical Wing.

chord line using a hydraulically driven rotary actuator located behind the wind-tunnel wall. Using this device, the model could be set at various mean angles, and the amplitude and frequency of oscillation could be varied.

An instrumentation layout for the wing is shown in figure 8. Unsteady pressures were measured along four chords at 30.9, 58.8, 80.9, and 95.1 percent of the 48-inch reference span. There were 14 measurement locations along each chord on the upper and lower surface of the wing and one location in the nose for a total of 29 pressure ports per wing chord. As shown in the figure, pressure measurements in the center section of the wing were made using both in situ transducers and matched-tube orifices. Pressures in the leading and trailing edges were acquired using only matched tube orifices. The matched tube orifices in the center of the wing adjacent to the in situ transducers were used to correct for the dynamic effects of the tubes in the forward and aft section of the wing.

Experimental Data Sets

The majority of test data were acquired in heavy gas, R-12, and these data are generally accepted as the most useful for CFD code validation and verification. The test conditions for which data was acquired are contained in the plot in figure 9. The RSW was tested at Mach numbers between 0.40 and 0.90, and static angles-of-attack between -4 and 14 degrees. The majority of data were acquired at angles-of-attack between -1 and 7 degrees. The high end of the Mach number and angle-of-attack range is well beyond the design point for this airfoil, but these conditions are representative of those that might be required for flutter verification beyond cruise conditions.

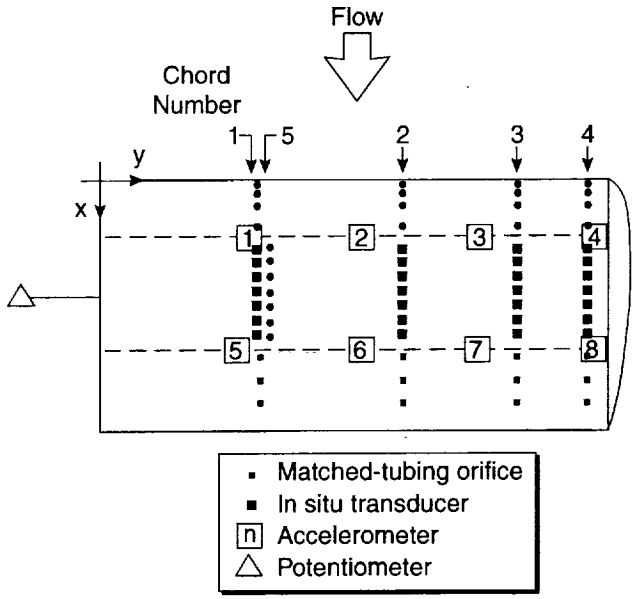

Fig. 8 Instrumentation layout for the Rectangular Supercritical Wing.

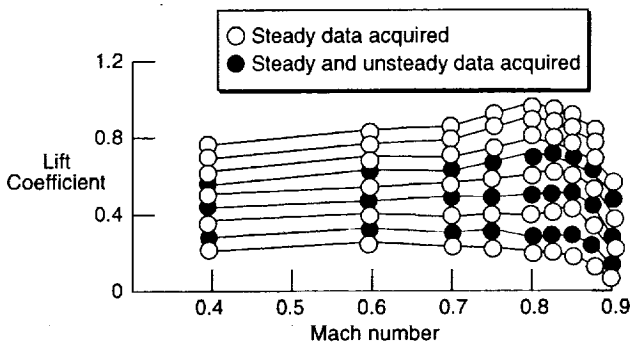

Fig. 9 Conditions where data was acquired during testing of the Rectangular Supercritical Wing.

Forced pitching oscillation data were acquired with amplitudes of 0.5, 1.0, and 1.5 degrees and frequencies of 5, 10, 15, and 20 Hz. Limited data is also available at frequencies below 5 Hz. Figure 10 shows a sample of the static pressure data acquired a Mach 0.802, and two degrees angle-of-attack. The figure shows the upper and lower surface pressure coefficient plotted as a function of fraction of wing chord at the 30.9 percent span station. A sample of the dynamic data acquired is presented in figure 11. In this figure, the top plot shows the real (in-phase) and imaginary (out-of-phase) components of the unsteady pressure for the upper surface orifices, while the bottom plot shows similar data for the lower surface. In both cases, the pressure components are further normalized by the amplitude of the pitching motion.

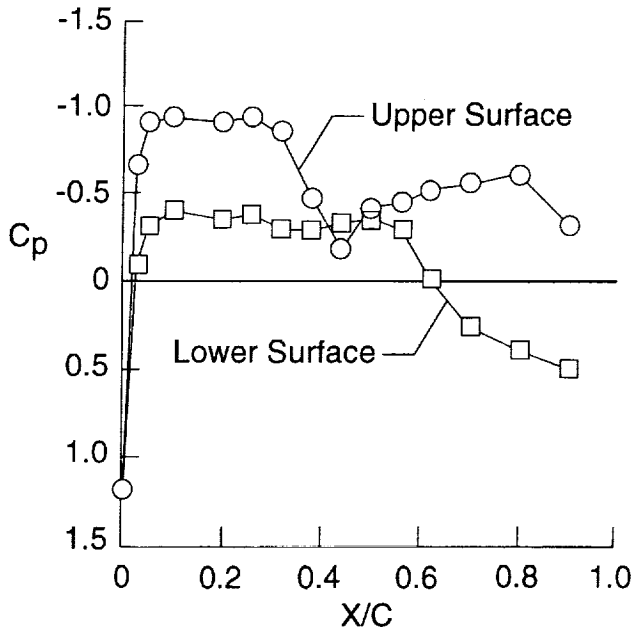

Fig. 10 Sample static pressure distribution for the Rectangular Supercritical Wing, $\eta = 0.309$, $\alpha = 2.0$ degrees, and $M = 0.802$.

Clipped Delta Wing

This investigation involved the measurement of unsteady pressures for a delta wing with a clipped tip undergoing rigid body pitching and trailing-edge control surface oscillations.[20,21] Bennett and Walker[22] documented the model geometry and experimental dataset for this wing in detail, and it has been selected as a test case for a NATO Research and Technology Organization (RTO) working group document on experimental and computational test cases for computational method validation.[18]

Physical Description

The wing planform was derived from a proposed design of a supersonic transport known as the Boeing 2707-300.[23] The leading-edge strake was removed from this configuration as were all camber and twist. The wing thickness was also increased to 6 percent of the chord from the typical 2.5 to 3 percent of the chord to accommodate instrumentation. The resulting airfoil was a circular arc profile. A layout of the wing planform and associated model instrumentation is shown in figure 12. Measured ordinates for this model are available in references 22 and 18.

Pressure instrumentation for this wing was located primarily on the upper surface. Lower surface pressure instrumentation was sparse and was only used to check model symmetry and angle-of-attack. As seen in the figure, there were four, well populated, rows of transducers designated as Chords A, B, D, and E. A fifth, less populated row, Chord C, was included to improve the resolution of data near the edges of the control surface. There were two orifices located at the majority of

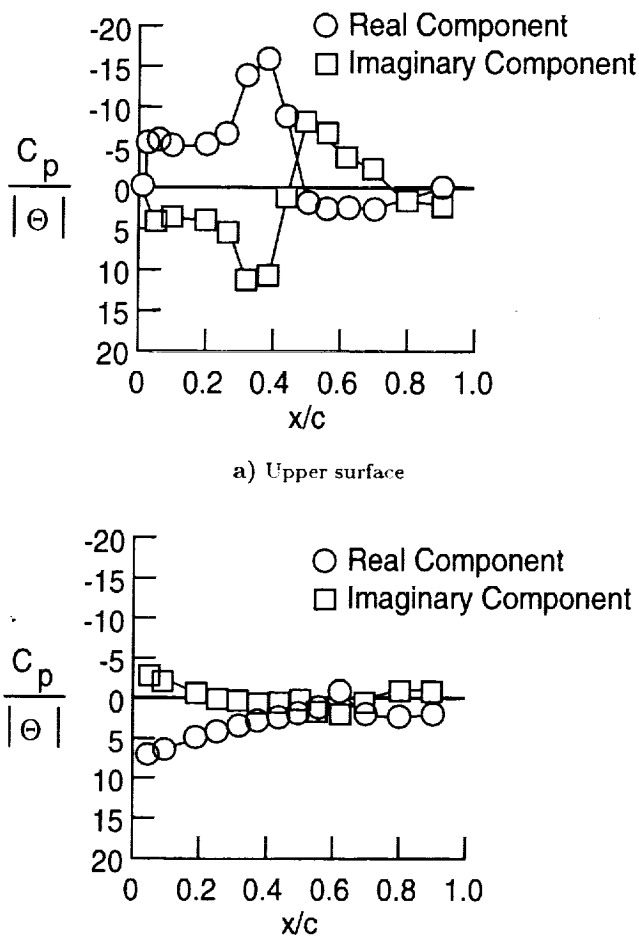

Fig. 11 Sample unsteady pressure distributions for the Rectangular Supercritical Wing, $\eta = 0.309$, $\alpha_{mean} = 2.08$ degrees, $\alpha_{amplitude} = 1.057$ degrees, $f = 9.96$ Hz, and $M = 0.804$.

locations represented by dots on the figure. One orifice was used to make static pressure measurements while the other was used for dynamic measurement with an in situ transducer. At locations near the wing trailing-edge that could not accommodate a transducer due to model volume constraints, only static pressure measurements were acquired.

The model is shown installed in the TDT in figure 13. It was mounted to a splitter plate that was offset from the TDT wall, and the root of the wing was attached to an endplate that moved with the wing during pitching oscillations. The model was oscillated in pitch using a large, hydraulically driven, spring system mounted behind the TDT wall. The mean angle-of-attack and the amplitude and frequency of pitch oscillation could be varied using this device. A miniature hydraulic actuator located in the wing drove the trailing-edge control surface.

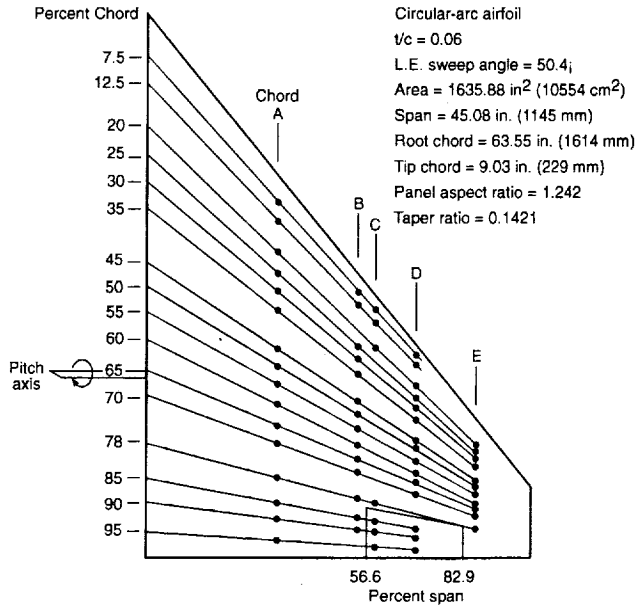

Fig. 12 Wing planform and instrumentation layout for the Clipped Delta Wing model.

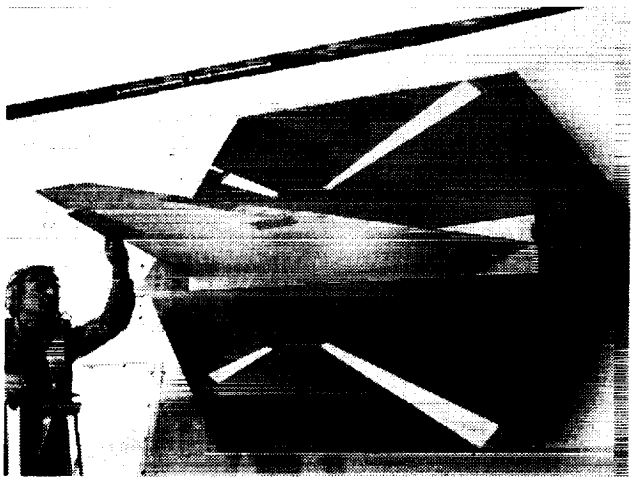

Fig. 13 Clipped Delta Wing model installed in the TDT.

Experimental Data

All tests were performed in heavy gas, R-12. Test conditions ranged from Mach 0.40 to 1.12 and static angles-of-attack from 0.0 to 5.5 degrees. The Reynolds number for this dataset is approximately 10 million based on the average wing chord. Forced pitch oscillation data were acquired at frequencies of 4, 6, and 8 Hz, and amplitudes of 0.25 and 0.50 degrees. Control surface oscillations were performed at frequencies of 8, 16, and 22 Hz with amplitudes of 2, 4, and 6 degrees. Sample static data from this test are plotted in figure 14. The pressures plotted on this figure are at the 54.1 percent span station, which is just inboard of the trailing-edge control surface. Figure 15 shows dynamic data at similar flow conditions and the same spanwise station. In this case, the wing has been oscillated at a frequency of 8 Hz with amplitude of 0.46

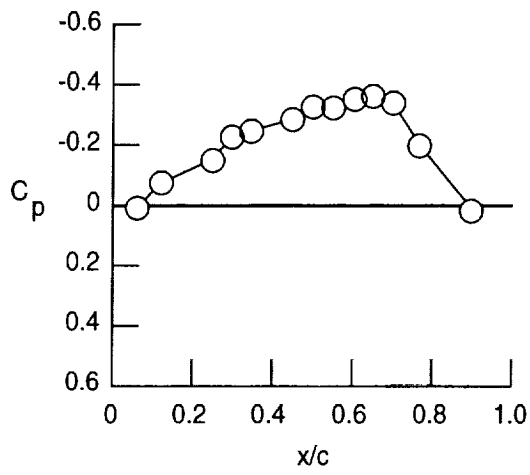

Fig. 14 Sample upper surface static pressure data for the Clipped Delta Wing, η = 0.541, α = 0.05 degrees, M = 0.90, and Re = 9.77 million (based on avg. wing chord).

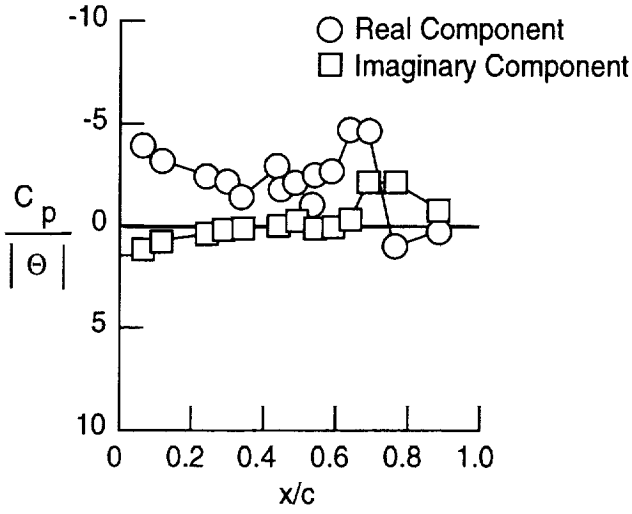

Fig. 15 Sample upper surface dynamic data for the Clipped Delta Wing, η = 0.541, α_{mean} = 0.0 degrees, $\alpha_{amplitude}$ = 0.46 degrees, M = 0.90, and Re = 9.77 million (based on avg. wing chord).

degrees about a mean angle-of-attack of zero degrees. Both the in-phase and out-of-phase components of the pressure coefficient normalized by the pitching amplitude are included in this figure. All data for the static and first harmonic unsteady pressure distributions are provided in reference 20, and selected cases are available in reference 18.

Benchmark Models

The NASA Langley Benchmark Models Program (BMP)[24] was established to provide experimental unsteady aerodynamics data, particularly at flutter conditions, specifically for computational method validation, verification, and evaluation. Stall flutter and plunge instability phenomena were also observed and studied in the BMP. The program focused on mak-

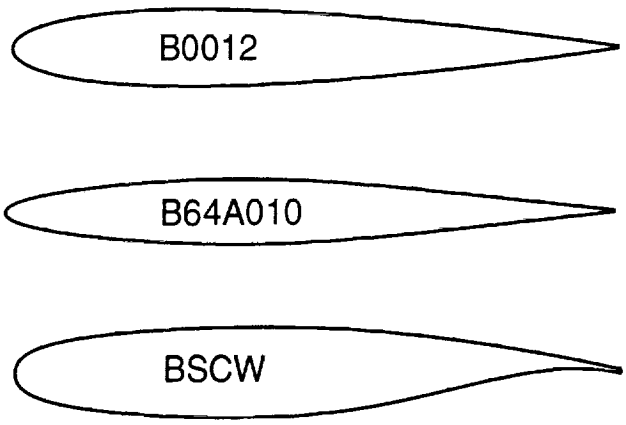

Fig. 16 Airfoil sections used to develop BMP models.

Fig. 17 BSCW model installed in the TDT.

ing very high quality unsteady pressure measurements on geometrically simple wings so as to simplify modeling in the computational methods and to facilitate the interpretation of results. Three wings[24-31] with the same rectangular planform were tested on a Pitch and Plunge Apparatus (PAPA)[32,33] at transonic test conditions. The model geometry and experimental datasets for these wings have been selected as a test case for a NATO Research and Technology Organization (RTO) working group document on experimental and computational test cases for computational method validation.[18]

Physical Description

Each wing had a different airfoil profile with different transonic performance characteristics. Figure 16 shows the airfoil profiles used to define the three models. The first Benchmark model was built using a NACA 0012 airfoil and was designated B0012. The second model, designated B64A010, used an NACA 64A010 airfoil, and the third model had an NASA SC(2)-0414 supercritical airfoil and was designated BSCW. The airfoils were chosen for their performance characteristics in transonic flow. These characteristics range from a strong, forward-positioned shock that is relatively insensitive to small changes in flow conditions on the B0012 to a weak, aft-positioned shock whose position is sensitive to flow conditions on the BSCW. The B64A010 was chosen because it had transonic characteristics that fall somewhere between the two extremes.

The three wing models were constructed and instrumented similarly, with slight differences in detail. They were fabricated in three parts to provide ready access to the instrumentation. Each had a rectangular planform with a span of 32 inches plus a tip of revolution. The chord for the three wings was 16 inches, giving the wings a panel aspect ratio of two. They were machined of aluminum to a very smooth finish. Detailed geometry measurements were performed for each of the wings along several sections so that as-tested geometries could be accurately modeled in computational methods.

Figure 17 shows the BSCW model installed in the TDT. The model was mounted on a large splitter plate offset from the wind-tunnel wall by approximately 40 inches. An end plate that moved with the model was attached to the root of the wing and moved within a recessed section of the splitter plate. A large fairing behind the splitter plate isolated the equipment between the plate and the sidewall from the tunnel flow.

These models were flutter tested using the Pitch and Plunge Apparatus (PAPA),[32,33] illustrated in the sketch of figure 18. The PAPA system permits rigid body pitch and plunge motions of the wing and flutter of the system by using four circular rods for flexibility. The rods are arranged such that the elastic axis is at the midchord and the model is balanced to place the center of gravity on the midchord. The system thus gives essentially uncoupled pitch and plunge modes about the midchord of the model.

In addition to the testing on the PAPA, the B0012 and BSCW models were tested on a rigid mount by locking the PAPA mechanism. These models could be pitched statically with the turntable, but there was no balance in this system for force measurements.

The models were instrumented for unsteady pressures and for dynamic motions at two chords. The primary dynamic motion measurements were made with the PAPA strain gages and accelerometers, although four wing accelerometers were included. There were 40 unsteady pressure transducers located along the chord at 60 percent span and 40 located at 95 percent span. The chordwise distribution of unsteady pressure transducers for the BSCW model is illustrated in figure 19, but was slightly different for each model.

Experimental Data Sets

The models were tested both in air and in heavy gas, R-12. TDT test conditions ranged from Mach

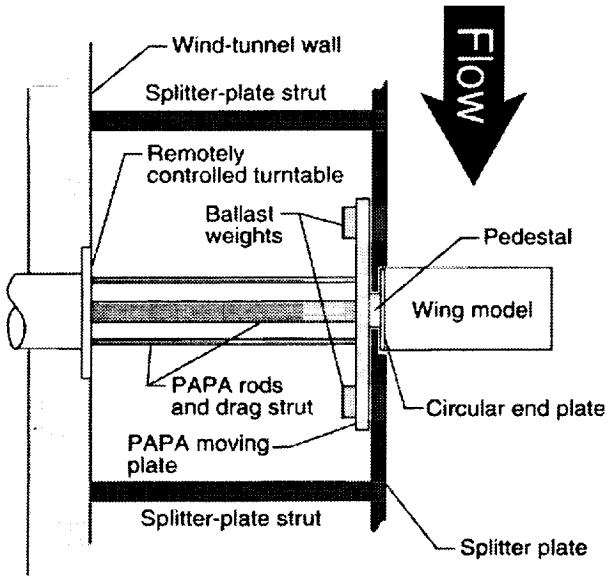

Fig. 18 Illustration of the BMP PAPA installation in the TDT.

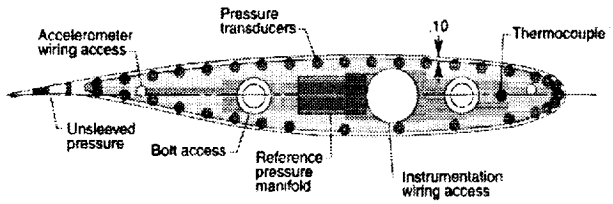

Fig. 19 Instrumentation installation in the BSCW model.

0.30 to 0.90 at angles-of-attack between -3 degrees and +5 degrees. Typical Reynolds numbers for these tests ranged between one and seven million based on the wing chord. The models were tested with both free and forced transition via a grit strip at 7.5 percent chord.

Static pressure data from the BSCW test are shown in figure 20. This plot shows the classical rooftop upper-surface pressure distribution with a terminating shock and the aft loading associated with supercritical airfoil technology. Figure 21 shows three plots describing the unsteady pressure distribution at 60 percent span on the BSCW acquired during flutter at a Mach number of 0.798. The top plot is the measured mean pressure distribution, which has similar characteristics to a supercritical airfoil at static conditions like that shown in figure 20. The middle and lower plots are the real (in-phase) and imaginary (out-of-phase) components of the pressure distribution as referenced to the pitching motion of the wing during flutter. For this case, the pitch frequency was approximately 5 Hz, and the pitch amplitude was 0.9 degrees. The real and imaginary components of the pressure clearly show the presence of a weak upper surface shock wave at these conditions.

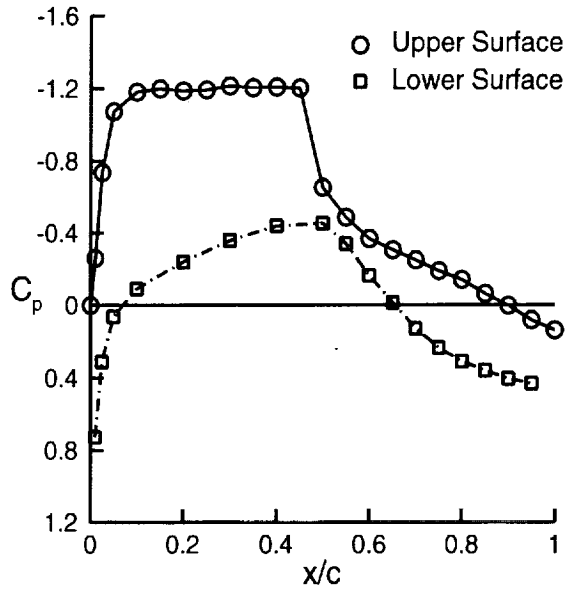

Fig. 20 Sample static pressure distribution measured on the BSCW model, $\eta = 0.60$, $\alpha = 4.83$ degrees, and $M = 0.802$.

Structural Model

The nominal measured structural characteristics of the BMP/PAPA systems are summarized in table 2. These parameters were obtained by measuring model masses and PAPA stiffness directly and performing ground vibration testing. For each of the BMP model and PAPA configurations, the PAPA stiffness and damping characteristics are identical, and the mass characteristics of each model were tuned via the ballast weights to give the same nominal mass properties and a center of gravity at the mid-chord.

Table 2 Measured nominal structural dynamic properties for BMP/PAPA.

	Plunge Mode	Pitch Mode
Frequency	3.33 Hz.	5.20 Hz.
Stiffness	2637 lb/ft	2964 ft-lb/rad
Damping Ratio	0.001	0.001
Generalized Mass	6.01 slug	2.78 slug-ft^2

Benchmark Active Controls Technology Model

The Benchmark Active Controls Technology (BACT) model[34,35] was developed under the Benchmark Models Program, described in the previous section, to acquire benchmark aerodynamic data with static and dynamic control surface deflections and to provide a testbed for active controls research. This model differed from the other BMP models in that it was fitted with three hydraulically actuated active control surfaces. A view of the BACT model

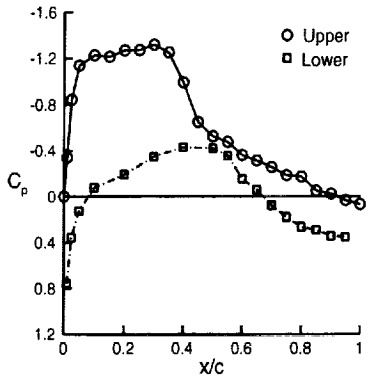

a) Mean Pressure Distribution

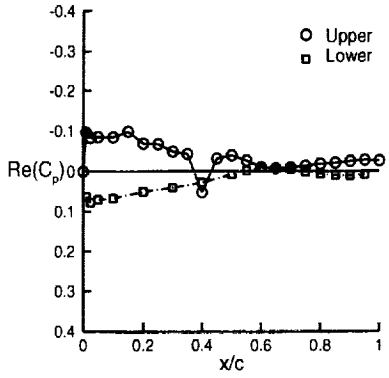

b) Real Component

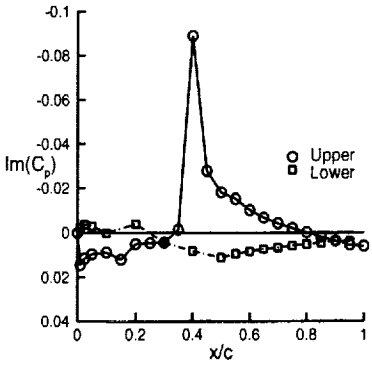

c) Imaginary Component

Fig. 21 Sample unsteady pressure distribution on BSCW model at flutter, $\eta = 0.60$, $\alpha_{mean} = 5.5$ degrees, and $M = 0.798$.

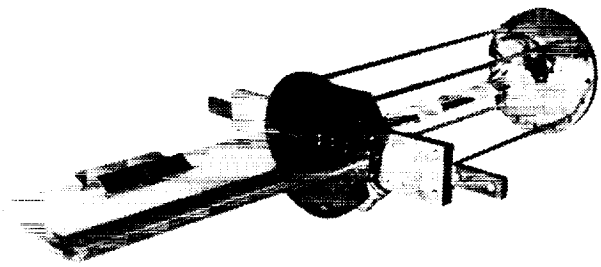

Fig. 22 BACT model mounted on the PAPA.

on the flexible (PAPA) mount is shown in figure 22. The model was based on the previously described B0012 model, which had a NACA 0012 airfoil. The BACT experimental data sets have been extensively used for computational aerodynamic, computational aeroelasticity, and aeroservoelastic (ASE) studies. Many of the papers which have used the BACT model and data will be highlighted in special sections of the Journal of Guidance, Dynamics, and Control. Currently these sections are scheduled to be published in the September-October 2000, November-December 2000, and January-February 2001 issues. Additionally, the model geometry and experimental dataset for this wing has been selected as a test case for a NATO Research and Technology Organization (RTO) working group document on experimental and computational test cases for computational method validation.[18]

Physical Description

The overall dimensions and geometry of the BACT model were the same as the B0012 model, as were the general construction techniques employed. The BACT model had a 25 percent chord trailing-edge control surface that extended between 45 and 75 percent span. It also had upper and lower surface spoilers of 15 percent chord, hinged at the 60 percent chord location and spanning the same distance as the trailing-edge control surface. The outer surface of the spoilers was flat with a relatively thin trailing-edge overlapping part of the round leading edge radius of the trailing-edge control surface. When both spoilers were deployed, the cavity underneath was open permitting flow between the upper and lower surfaces. The control surfaces were of composite construction and were driven with miniature hydraulic actuators located in the wing.

The model was instrumented for unsteady pressures at two chords. The orifice layout at the 40 and 60 percent span station is shown in figure 23. There were 58 unsteady pressure transducers located along the chord at 60 percent span, which is the midspan of the control surfaces. There were 5 transducers on each spoiler and 7 on each of the upper and lower surfaces

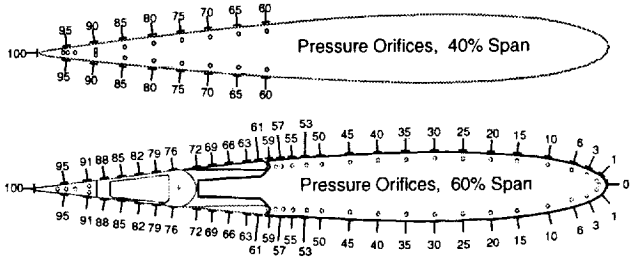

Fig. 23 BACT pressure orifice layout.

of the trailing-edge control surface. This relatively dense spacing of the transducers was selected to define the pressures near the control surface hinge lines. In addition there were 17 unsteady pressure transducers located at 40 percent span over the aft portion of the chord that were placed to examine the carry-over loading near the side edge of the control surfaces. Space limitations prevented further pressure instrumentation at other chords.

The model was mounted on the same splitter plate as that used in the previous BMP tests. The BACT model was tested on both a rigid strut equipped with a 5 degree-of-freedom balance and the PAPA.[32,33] On both devices the static angle-of-attack could be controlled via a turntable located behind the wind-tunnel wall.

Experimental Data Set

An extensive experimental dataset has been acquired on the BACT wing. The majority of testing was performed in the heavy gas, R-12, but limited data were also acquired in air. Static cases included variation of Mach number and angle-of-attack for the baseline configuration, static deflection of each of the individual control surfaces at a variety of Mach numbers and angles-of-attack, and static deflections of combinations of control surfaces. Dynamic data was also acquired with the model mounted on the rigid strut by oscillating individual control surfaces at a variety of frequencies, amplitudes, and mean deflections. Both flutter data and forced response data were acquired with the model mounted on the PAPA. In general, the model was tested at Mach numbers between 0.63 and 0.94 at angles-of-attack ranging from -4 to +10 degrees. Trailing-edge control surface static deflections ranged from -10 to +12 degrees, and spoiler deflections varied between 0 and 40 degrees. Control surface oscillations were accomplished at frequencies up to 10 Hz, and amplitudes of 1, 2, and 4 degrees for the trailing-edge control surface and up to 10 degrees for the spoilers. Transition was fixed at five percent chord on both the upper and lower surfaces using a grit strip.

A sample of unsteady pressure data acquired during a trailing-edge control surface oscillation is shown in figure 24. The flow conditions for this case were Mach 0.77 and 4.0 degrees angle-of-attack and the data are for the 60% span station. The top figure presents the mean pressure coefficient along the wing chord. The middle and bottom figures show the real (in-phase) and imaginary (out-of-phase) pressure components, respectively, referenced to the trailing-edge control surface motion. In these plots, the shock motion is clearly identifiable in the unsteady pressures, as is the pressure disturbance at the hinge line of the control surface.

Three types of instabilities were encountered with the BACT/PAPA system. One was a classical flutter instability where the two primary vibratory modes coalesce. The other instabilities were a plunge instability and a stall instability. The tunnel conditions where instabilities occurred are shown in figure 25. The boundaries where these instabilities occurred are similar to the ones encountered in the previous B0012 model test described in reference 26. Time history data were acquired at most of these points and magnitude and phase of pressures were calculated at the frequency of the instability.

The classical flutter boundary for the BACT model is represented by the circular symbols in figure 25. The open-loop model is stable below this boundary and unstable above. This boundary was obtained with zero bias on the control surfaces and an angle of attack large enough to create lift approximately equal to weight of the model. There is a transonic dip near M=0.77 followed by a sharp upward turn of the boundary near M=0.8. For the M=0.63 and q=158 psf flutter point, magnitude and phase of unsteady pressures at the flutter frequency of 4.3 Hz are shown in figure 26. The zero magnitude data points in figure 26 correspond to transducers that were no longer functioning.

Occurrences of a plunge instability are indicated by the square symbols in figure 25. This instability occurs in a narrow transonic Mach number range around 0.92 and consists primarily of the plunge mode at a frequency around 3.5 Hz. Since this instability is caused by the fore and aft motion of symmetric shocks on the upper and lower surface of the wing, it is very sensitive to any biases and does not occur with nonzero control surface bias or nonzero alpha.

Occurrences of stall flutter are indicated by the diamond symbols in figure 25. This instability is caused by wing stall occurring during a portion of the pitch oscillation cycle. The primary mode in this instability is the pitch mode at a frequency around 5 Hz. This instability could be encountered at most tunnel conditions where high angles of attack could be attained without exceeding the load limits for the PAPA mount. Generally stall flutter was encountered at mean angles exceeding 4 degrees.

Below the classical flutter boundary, control surface inputs were used to excite the BACT model so that frequency response functions could be calculated and compared with results of aeroservoelastic codes. An

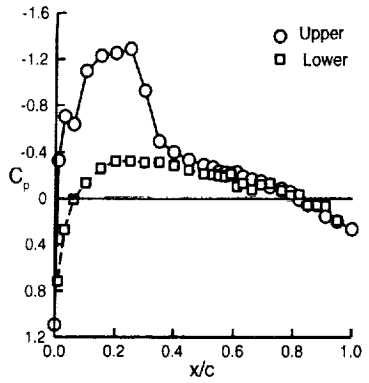

a) Mean Pressure Distribution

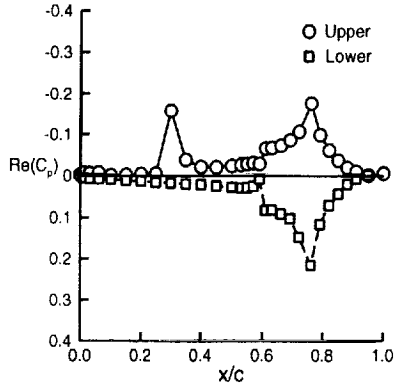

b) Real Pressure Component

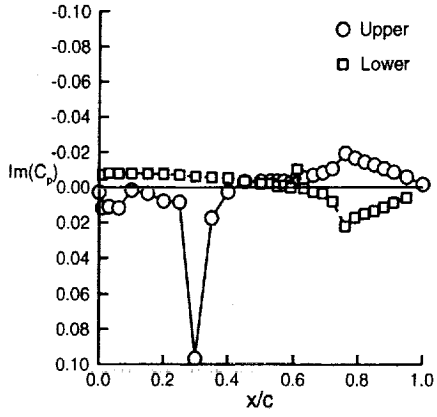

c) Imaginary Pressure Component

Fig. 24 Sample unsteady pressure data acquired on the BACT model, $\eta = 0.60$, $\alpha = 4$ degrees, and $M = 0.77$.

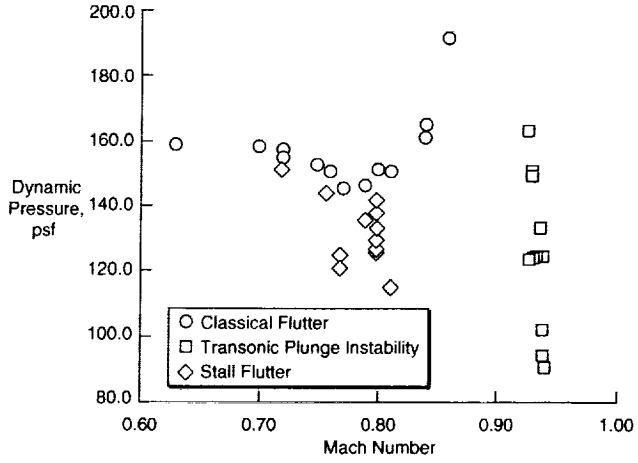

Fig. 25 BACT instabilities.

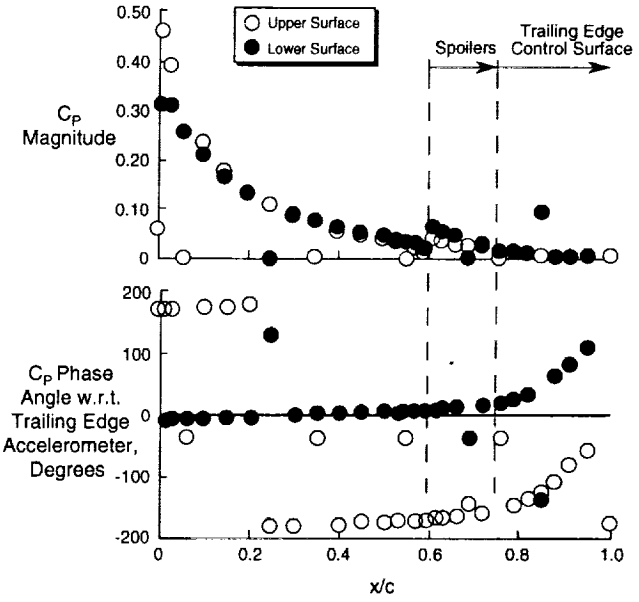

Fig. 26 Unsteady pressures at 60% span acquired during flutter on the BACT model, M = 0.63, and q = 158 psf.

example frequency response function for spoiler input and trailing edge accelerometer output is shown in figure 27. Here, both spoilers were biased 10 degrees into the airstream, and their input was a linear sine sweep. Note that for this condition, the two primary modes of motion, pitch and plunge, still exist as distinct modes as indicated by the separate peaks in the magnitude plot at about 3.4 and 4.6 Hz, respectively. Reference 36 made extensive use of these data to compare with aeroservoelastic models of the BACT plant.

Structural Model

The structural characteristics of the BACT/PAPA system are summarized in table 3. The mass and stiffness parameters were measured directly, GVT analyses were performed to determine frequencies and damping characteristics.

A simulation model of the BACT plant was de-

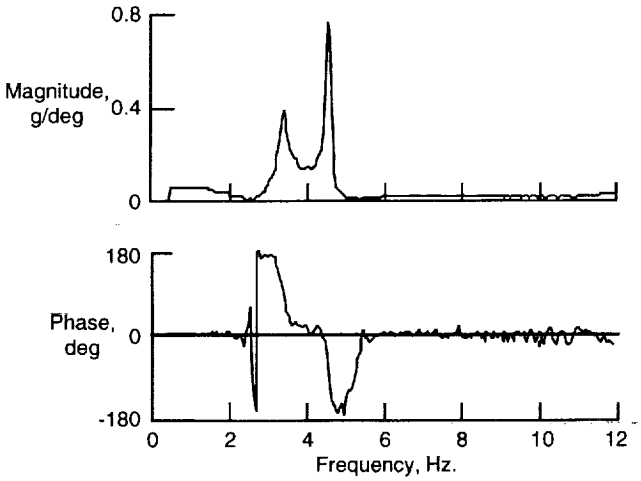

Fig. 27 Acceleration frequency response function due to upper and lower spoiler position (US+LS) for the BACT model, M = 0.65, and q = 114 psf.

Table 3 Measured structural dynamic properties for BACT/PAPA.

	Plunge Mode	Pitch Mode
Frequency	3.34 Hz.	5.21 Hz.
Stiffness	2,686 lb/ft	3,000 ft-lb/rad
Damping Ratio	0.0014	0.0010
Generalized Mass	6.08 slug	2.80 slug-ft^2

veloped by Waszak.[36,37] The model was formed by combining the aeroelastic equations of motion for the BACT wind-tunnel model with actuator models and a model of wind-tunnel turbulence. Wherever possible, the simulation model parameters were determined experimentally. The static aerodynamic parameters were determined from experimental data when the BACT model was mounted to a five-degree-of-freedom balance.[35] The dynamic derivatives were obtained computationally using ISAC.[38] The numerical values for the static and dynamic stability and control derivatives are only valid at a single Mach number of 0.77; however, the dynamic pressure for the simulation model could be changed.

Aerodynamic Models and Investigations

Several studies have compared computational results with BACT experimental data.[18,39] In one study a comparison of results for a fixed and oscillating spoiler was made with the BACT data.[39] Steady pressure coefficients at span locations of 40% and 60% with the upper spoiler deflected 15 degrees are shown in figure 28. Figure 29 compares the computed real and imaginary unsteady pressure coefficients for an oscillating spoiler case with experiment.

In another study, computations for deflected and oscillating aileron were compared with the BACT data.[39] Results presented were at Mach number of 0.77, at static deflections of 5 and 10 degrees for the steady

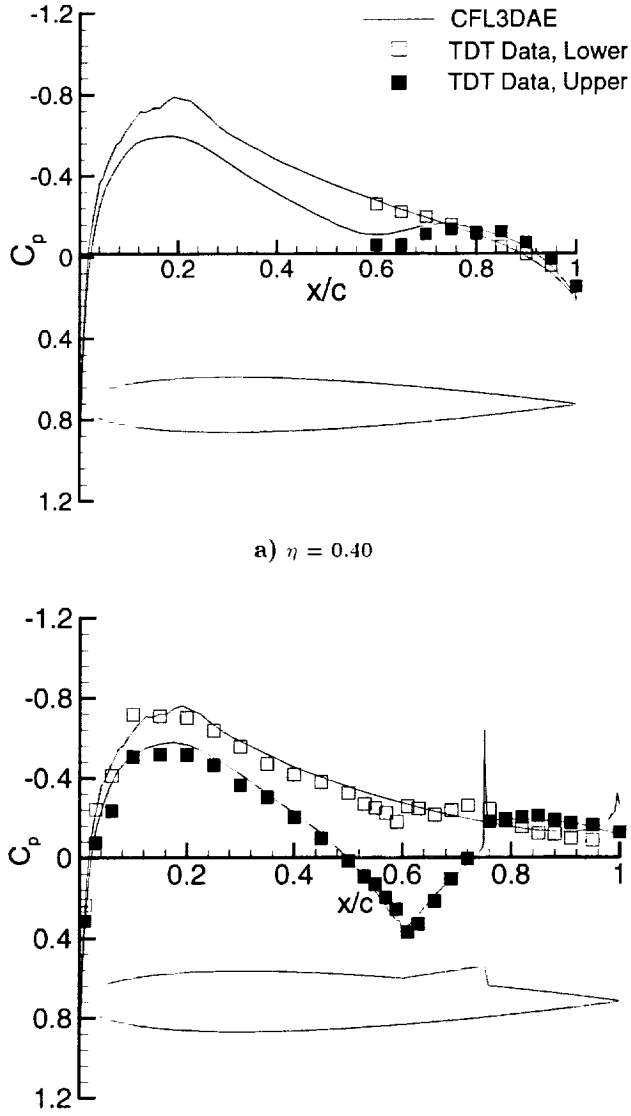

Fig. 28 Comparison of measured and computed BACT model steady pressure coefficients, M = 0.77, α = 0 degree, δ_{US} = 15 degrees.

cases, and amplitudes of 2 degrees at 5 Hz for the unsteady cases. Each of these analyses offered reasonable comparison with the experimental data, while at the same time revealing some of the deficiencies in the idealized continuous surface modeling used in the simulations.

Aeroelastic Research Wing - 2

In NASA's Drones for Aerodynamic and Structural Testing (DAST) program[40] two elastic supercritical wings were designed to be flight-tested on an unmanned remotely-piloted drone aircraft. The purpose of the program was to provide a complement to wind tunnel and full-scale piloted flight-testing of realistically flexible structures, allowing investigation of active control concepts such as flutter suppression, gust alleviation, and maneuver load control. A delay and

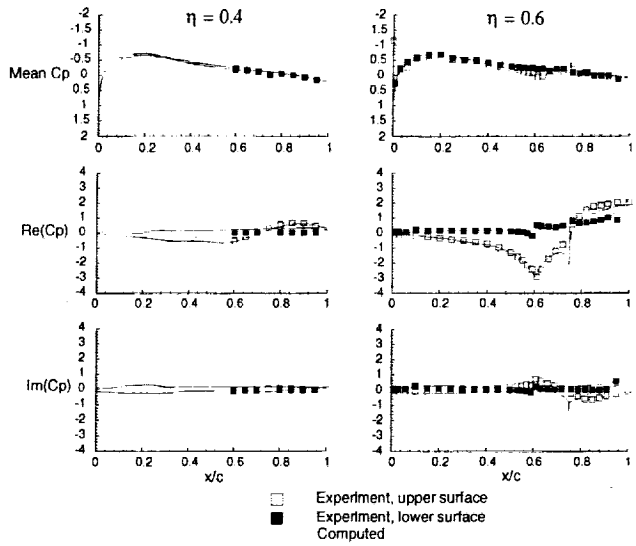

Fig. 29 Comparison of BACT model unsteady pressure coefficients due to upper spoiler oscillation, M = 0.77, δ_{USmean} = 5 degrees, $\delta_{USamplitude}$ = 4.5 degrees, f = 9.56 Hz, and k = 0.1088.

eventual cancellation of the flight test program of the second Aeroelastic Research Wing (ARW-2) made the right wing panel available for testing in the Transonic Dynamics Tunnel. Although the design flutter boundary was outside the tunnels operational boundary, the availability of the unsteady pressure transducer instrumentation and hydraulically actuated aileron control surface made this an attractive test.

Physical Description

Figure 30 shows the right wing panel installed on the tunnel sidewall on a half-body fuselage used to simulate the drone fuselage. Both the fuselage and the wing were mounted on the remotely controlled turntable mechanism located on the tunnel sidewall. The wing had an aspect ratio of 10.3 and a leading-edge sweep of 28.8 degrees. It was equipped with three hydraulically driven control surfaces, two inboard and one outboard aileron. The inboard surfaces were held fixed at 0-degrees and only the aileron was deflected statically and dynamically. The wing contour was formed by blending three different supercritical airfoil shapes one at the wing-fuselage junction, another at the wing planform break, and the third at the wing tip. The three sections had thickness-to-chord ratios of 0.15, 0.12, and 0.11 respectively. The wing construction jig shape was derived from the defined cruise Mach number of 0.80, the corresponding loading conditions, and the flexibility of the wing structure. Geometric (including ordinate measurements) and structural details of the model are detailed in reference 41. Airfoil ordinates have recently been edited, smoothed, and interpolated for a better CFD definition.

The locations of the wing instrumentation are shown in figure 31. The instrumentation consisted of 191

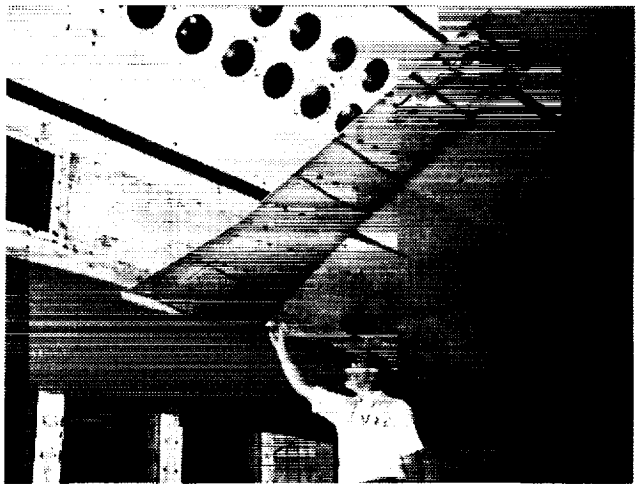

Fig. 30 ARW-2 wing mounted on east wall of the TDT.

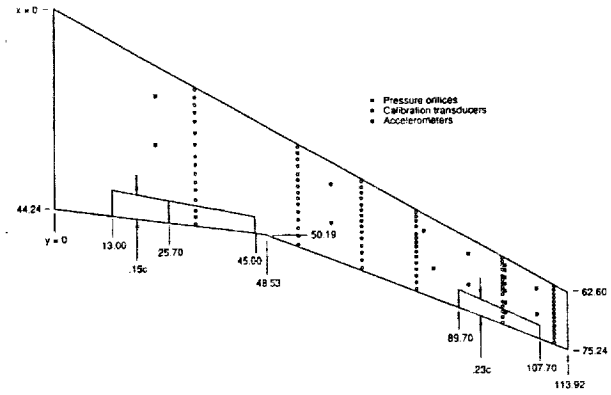

Fig. 31 Planform, control surface, and instrumentation layout for the ARW-2 wing.

pressure transducers and 10 accelerometers. In addition, strain gages were located near the wing root to measure bending moments. The model angle-of-attack was measured by a servo accelerometer that was mounted near the wing root. Both steady and unsteady pressures were obtained using differential pressure transducers referenced to tunnel static pressure. Streamwise rows of upper and lower surface pressure orifices were located at six span stations shown in the figure.

Experimental Data Sets

Two tunnel tests of the model were conducted in 1983 and 1985. The matrix of wind-tunnel test conditions for the steady pressure measurements during the first test is shown in figure 32. Test Mach numbers included 0.60, 0.70, 0.75, 0.80, 0.85, and 0.88. At a dynamic pressure of 100 psf, the Reynolds number (per foot) varied from 1.7 to 2.5 million at Mach numbers of 0.6 to 0.9. Measurements were made along lines of constant tunnel stagnation pressure. Additional measurements were made for tunnel dynamic pressures of 100 and 200 psf. where unsteady pres-

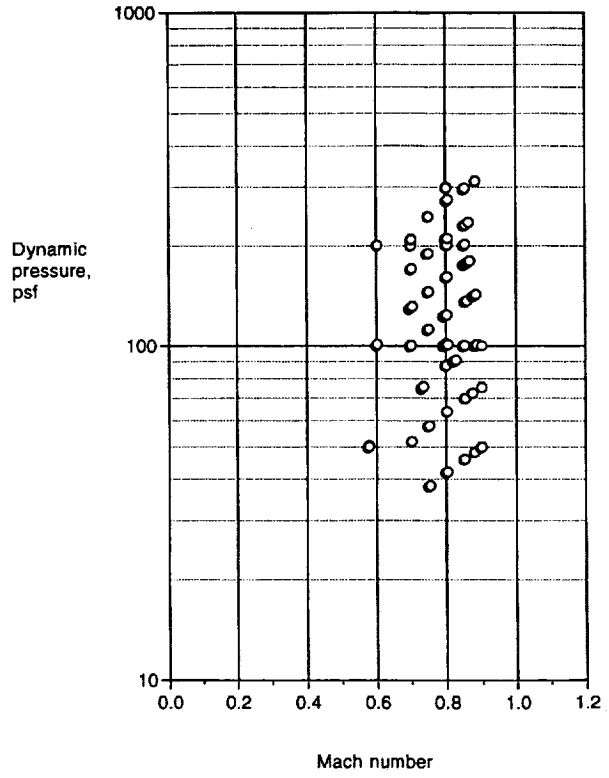

Fig. 32 TDT test condition matrix for the ARW-2.

sures were measured. Reference 42 summarizes results from the first test. The steady pressure data from this test are reported in reference 43. Model configuration variations included angle of attack values from -2 to +4 degrees and aileron deflection angles from -8 to +8 degrees. An outstanding feature of this test was the extensive photogrammetric measurement of the wing static deflections for these conditions.[44] Figure 33 and figure 34 show representative steady chordwise pressures for varying span stations at M = 0.80 and varying Mach number at span station 0.87, respectively.

Also during this first test, unsteady pressures were measured while oscillating the outboard aileron control surface and the data is reported in Reference 45. Tunnel conditions were Mach numbers of 0.60, 0.70, 0.80, and 0.85 and dynamic pressures of 100 and 200 psf. Model configuration variations included angles-of-attack of 0 and 2 degrees, dynamic aileron deflection amplitudes of 1, 2, and 3 degrees about a mean deflection of 0 degrees, and aileron oscillation frequencies of 5, 10, and 15 Hz. Figure 35 shows the effect of Mach number on the magnitude and phase of the unsteady lifting pressure at span station 0.87. The effect of the upper surface shock motion induced by the aileron oscillations is clearly seen in the lifting pressure magnitude for M=0.70, 0.80, and 0.85.

During this first test, a region of high wing dynamic response was observed near M=0.90 which persisted over the complete dynamic pressure range of the tunnel.[42] The wing motion was predominantly in the wing

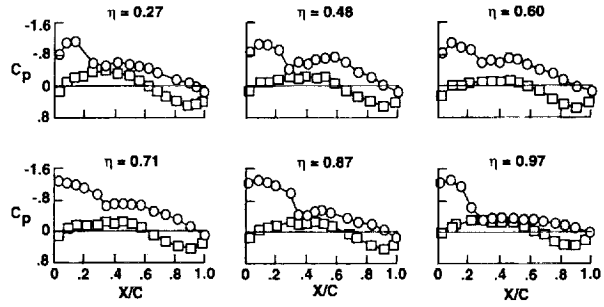

Fig. 33 ARW-2 steady pressure distributions at six span stations, M = 0.8.

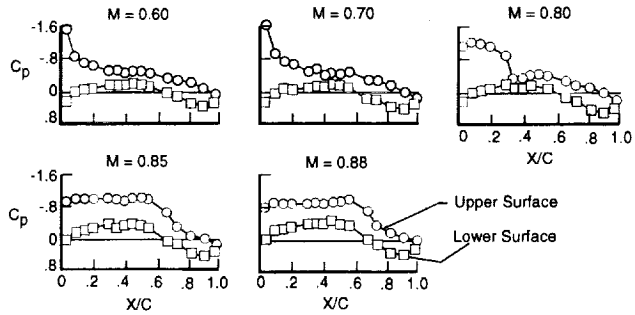

Fig. 34 ARW-2 steady pressure distributions at five Mach numbers, η = 0.87.

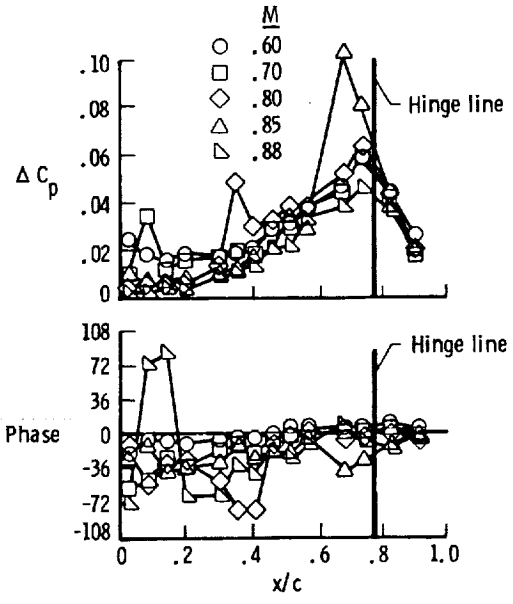

Fig. 35 Unsteady lifting pressure distribution due to aileron oscillation as a function of Mach number for the ARW-2 wing, η = 0.87.

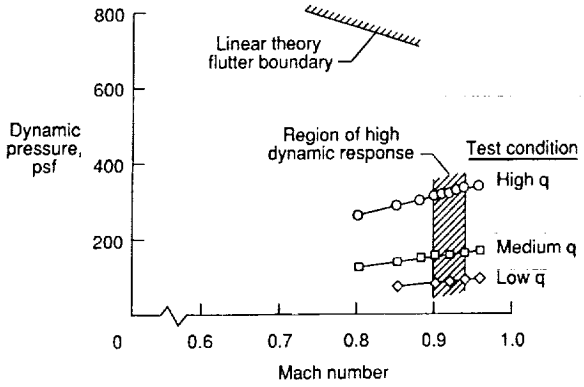

Fig. 36 ARW-2 test envelope and regions of high dynamic response.

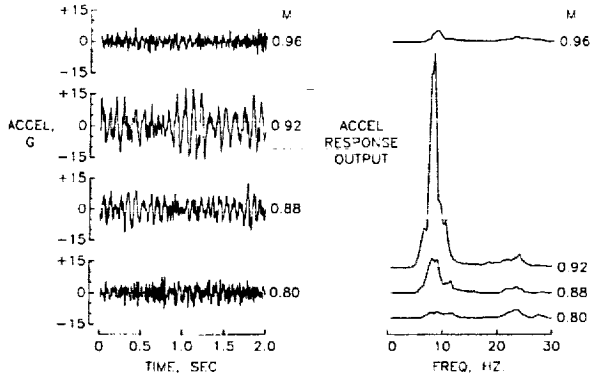

Fig. 37 ARW-2 accelerometer time history and frequency response data.

first bending mode, with the frequency varying from 8.6 Hz at the lowest dynamic pressure to about 13 Hz at the highest dynamic pressure. The first bending mode wind-off frequency was 8.3 Hz. It was this wing response which limited testing to M = 0.88 or less during the first tunnel test. Subsequent interest in this "single-degree-of-freedom" type response resulted in the second tunnel test of the model in order to study the unsteady loading involved. Results of this second test are reported in references 46–48.

Figure 36 indicates the region of high-dynamic response that was measured during this test. (In references 42 and 46 the region is erroneously labeled as an "instability boundary.") The region is well below the calculated linear theory flutter boundary of the wing (in air). Three traverses of the region for increasing values of tunnel stagnation (and dynamic) pressure were made. Figure 37 shows accelerometer time history and frequency analysis results for increasing Mach number. Maximum response amplitudes occur near $M = 0.92$ and the response subsides by $M = 0.96$. The maximum wing response level increased with increasing dynamic pressure. Figure 38 shows upper and lower surface pressure time histories and mean pressure distributions at span station 0.87 for four Mach numbers bracketing the high response

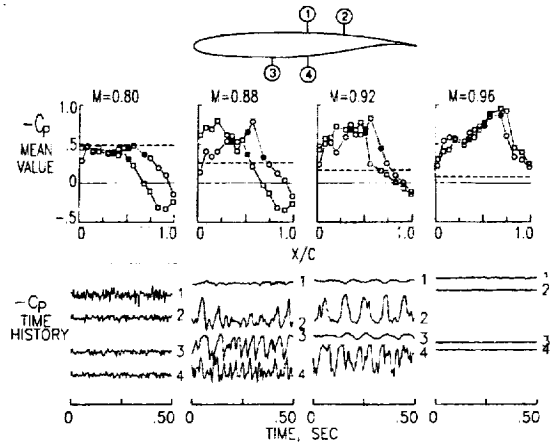

Fig. 38 ARW-2 mean pressure distributions and selected unsteady pressure time histories as a function of Mach number.

region. Reference 46 discusses the interpretation of such mean pressure distribution data in light of surface tuft studies that were also conducted during the test. A significant observation is that the tuft studies clearly indicated regions of intermittent flow separation at conditions where this was difficult to discern from the mean pressures. Reference 48 is a comprehensive report of the unsteady pressures measured in this test. The nature of the wing response is certainly that of buffet onset and is due to the initiation of flow separations on the upper and lower surfaces. Unsteadiness in the wing loading drives the wing primarily in its first bending mode somewhat akin to the "torsional wing buzz" reported in reference 49.

Structural Model

Several structural models of the ARW-2 have been created since the 1980's. During the original finite element model (FEM) development, the important model components were weighed, tested statically and dynamically, and modeled individually with the results correlated to experiment. Reference 41 describes the geometric and structural properties of the ARW-2 wing including the original structural model created using the SPAR[50] (Structural Performance and Resizing) code. This original model was later converted to EAL[51] (Engineering Analysis Language), and a simplification of the model was later made with EAL version 325. This simplification was to eliminate the extensional-bending coupling and off-diagonal bending terms in the skin composite stiffness matrices. Also, the diagonal bending terms were assigned a nominal value and tuned to give essentially the same results as the original model. Recently, the simplified EAL model was converted to an MSC/NASTRAN model. The MSC/NASTRAN FEM is a direct translation of the simplified EAL model, and is described in reference 52. The results obtained using the NASTRAN FEM correspond well with those in reference 41. These

structural models are available for distribution.

Aerodynamic Models and Analyses

Reference 53 describes a study that utilized the ARW-2 data set. In this study computational simulations were performed using an aeroelastic code, ENSAERO, which computes the unsteady aerodynamics and structural dynamics of the wing using strong conservation-law form of the thin-layer Reynolds-averaged Navier-Stokes equations for the fluid flow and modal or finite element equations for the structures. Static aeroelastic cases agreed well with experimental data for both aerodynamic load distributions as well as static displacements. Unsteady, dynamic aeroelastic computations were able to capture the sustained structural oscillations observed experimentally.

High Speed Research Rigid and Flexible Semispan Models

Under the NASA High-Speed Research (HSR) program, a series of wind-tunnel models were developed to acquire static and dynamic pressure data for configuration and computational code evaluation.[54] These models, known as the HSR Rigid Semispan Model (HSR-RSM) and the HSR Flexible Semispan Model (HSR-FSM), were virtually identical in geometry and instrumentation. The HSR-RSM is a very stiff model to minimize aeroelastic deflections, while the HSR-FSM was designed with a flexible structure aeroelastically scaled to anticipated flight vehicle specifications.

Physical Description

The wings for these models were patterned from an existing High Speed Civil Transport (HSCT) planform known as Reference H. Figure 39 shows the wing planform and instrumentation layout for these models. To accommodate instrumentation in the wing tip area, the airfoil sections were scaled to be four percent thick over the entire wing planform. The models were constructed using composite materials that consisted of a foam wing core with graphite epoxy (RSM) or fiberglass (FSM) skins bonded to the core. Rigid fuselage fairings were constructed for the models to serve two purposes. First they displaced the wing sufficiently far from the wind-tunnel wall so that the wing root would not be in the tunnel wall boundary layer. Second, they provided a realistic aerodynamic boundary condition at the wing root.

The models were mounted to a turntable located behind the east wall of the TDT that was used to control the model angle-of-attack. A variety of attachment devices were used to mount the models to the turntable. Both models were tested on a balance as shown in the figure. The HSR-RSM was also tested on a Pitch and Plunge Apparatus (PAPA)[32,33] to simulate rigid-body, two-degree-of-freedom dynamics on the model. The HSR-FSM was only tested on the balance for subcritical conditions. A rigid strut replaced the balance

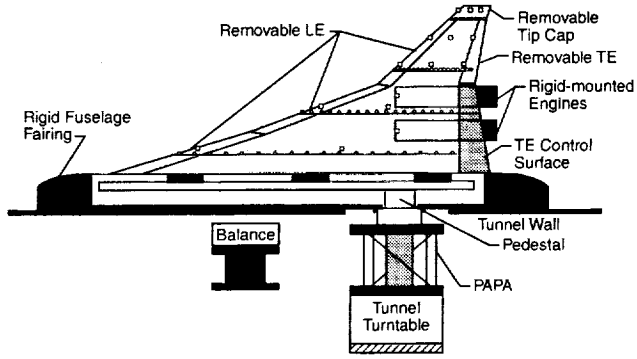

Fig. 39 Wing planform and instrumentation layout for the HSR-RSM and HSR-FSM models.

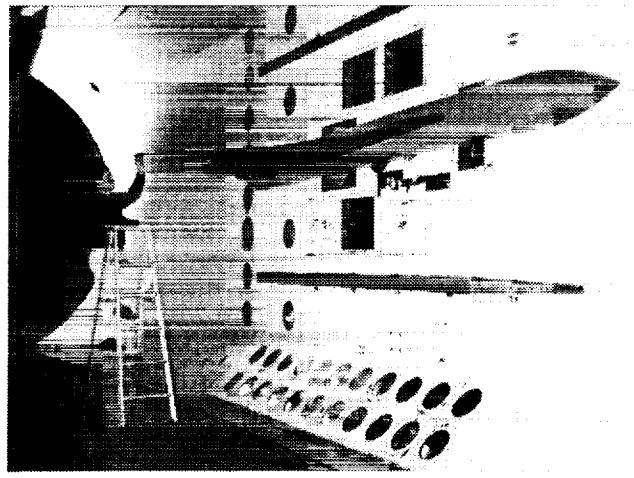

Fig. 40 HSR-RSM model mounted in the TDT.

for flutter testing. The HSR-RSM, as it was mounted in the TDT, is shown in figure 40.

The primary purpose of tests on these models was to acquire unsteady wing pressure data for correlation with theoretical analysis and design methods under development in the HSR program. Each model had 131 in situ unsteady pressure transducers distributed in chordwise bands at the 10, 30, 60, and 95 percent span stations. Each model could also be tested with or without a pair of flow-through nacelles and both had a hydraulically actuated inboard trailing-edge control surface that could be oscillated to generate unsteady aerodynamics data. In addition to the dynamic pressure instrumentation, the wings also had 14 accelerometers distributed throughout the wing planform, and the rigid fuselage fairing was instrumented with 120 steady pressure orifices at seven fuselage stations. Since the HSR-FSM was a structurally flexible wing, it included one torsion strain gage and three bending strain gages in its instrumentation suite and photogrammetric deflection measurements were also performed on the wing tip.

Experimental Database

The HSR-RSM and HSR-FSM were tested in the spring of 1996 using R-12 as the test medium. The HSR-RSM was subsequently tested on the PAPA in

the fall of 1998 using R-134A as the test gas. Large steady and unsteady force and pressure databases[55,56] were acquired for all three tests. Steady and unsteady data were obtained on these models in the form of angle-of-attack polars, steady flap deflection polars, and forced dynamic responses due to flap deflections. These data are summarized in table 4 for the three test entries. Due to dynamic constraints, a second, significantly shorter fuselage fairing was constructed for the HSR-RSM model when it was mounted to the PAPA. Therefore, much of the static data acquired during the first tunnel entry of the HSR-RSM was repeated for the PAPA test by initially mounting the model on a rigid strut. The PAPA data described in the table were all acquired on this rigid strut.

Typical pressure distributions obtained on the HSR-RSM and the HSR-FSM are shown in figure 41. This plot of the 60 percent span pressure coefficient versus nondimensional local streamwise coordinate at Mach 0.95, 2 degrees angle-of-attack, and a dynamic pressure of 150 psf clearly shows the effect of static aeroelastic deflections between the HSR-RSM and the HSR-FSM. In addition to the pressure data available in table 4, unsteady pressures were also measured at or near flutter for the HSR-FSM and the HSR-RSM on the PAPA.

Figure 42 summarizes results from the HSR-FSM testing showing areas of high model dynamic response and flutter. The squares in the figure represent points where forced response data were acquired by first identifying the dominant structural frequency at the given Mach number/dynamic pressure condition then oscillating the trailing-edge control surface at this frequency to obtain the response. A region of high dynamic response was identified in the high transonic Mach number range and is depicted by the dark shaded area in the figure. This area was characterized by an increased response of the first bending mode at a frequency of approximately 8.5 Hz. While high levels of dynamics were encountered in this region, flutter was not observed. A second area of high dynamic response is labeled as the "chimney" in the figure. In this area, the dominant response frequency ranged between 11.9 Hz and 14.0 Hz, significantly higher than the first wing bending mode. A hard flutter point was encountered in this region, at the conditions shown on the figure, which resulted in the catastrophic failure of the model structure. Despite this, a significant amount of unsteady pressure data was acquired in and around the various areas of high dynamic response that should prove very useful in understanding the aeroelastic characteristics of this wing.

Finally, the HSR-RSM model tested on the PAPA provides two-degree-of-freedom flutter data at a frequency of approximately 4.75 Hz. HSR-RSM/PAPA flutter boundaries are shown in figure 43. The sensitivity of the flutter boundary to variations in angle-of-attack was evaluated during this test. These data

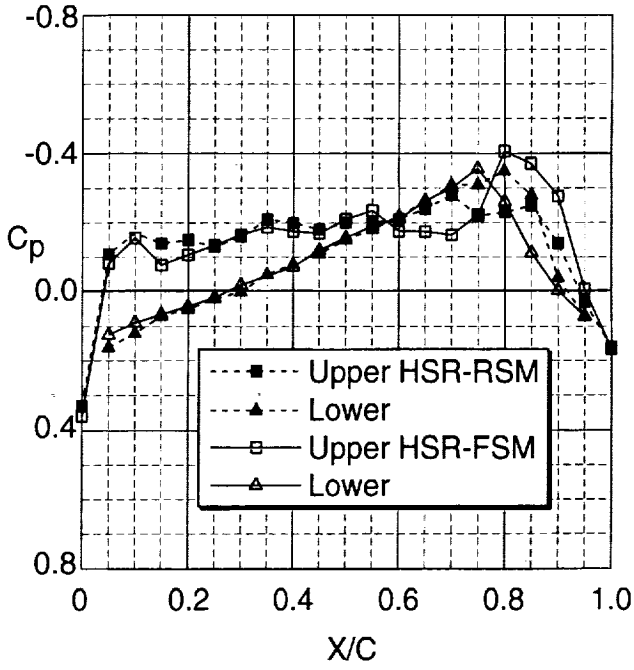

Fig. 41 Rigid/Flexible pressure comparison at 60% span for HSR models at M = 0.95, α = 2.0, q = 150 psf.

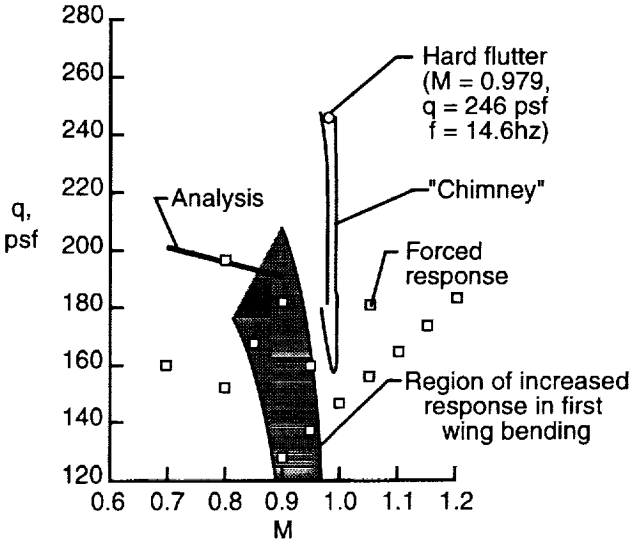

Fig. 42 Experimentally observed regions of high dynamic response and flutter for the HSR-FSM model.

showed the model to be unexpectedly sensitive to changes in angle-of-attack suggesting that strong nonlinear effects, aerodynamic and/or structural, were present during these tests.

Structural Model

As with the BMP/PAPA configurations, the RSM/PAPA is a relatively simple structure to model analytically. However, unlike the BMP models, the RSM was tested in several configurations each having unique mass and inertia properties. For this reason a

Table 4 **HSR-RSM/FSM TDT test data summary.**

Model	Mach Range	Dynamic Pressures (psf)	Steady Data	Forced Oscillation Data
RSM/Balance	0.7 - 1.15	100, 150, 200	α = -3 - +8 δ = -5 - +5	δ = 2, 5 f = 1, 2, 5 Hz
FSM	0.8 - 1.15	100, 125, 150	α = -1 - +2.5 δ = -4 - +4	Various Combinations
RSM/PAPA	0.6 - 1.10	150	α = -5 - +5	δ = 0.25, 1 f= 1, 5, 10 Hz

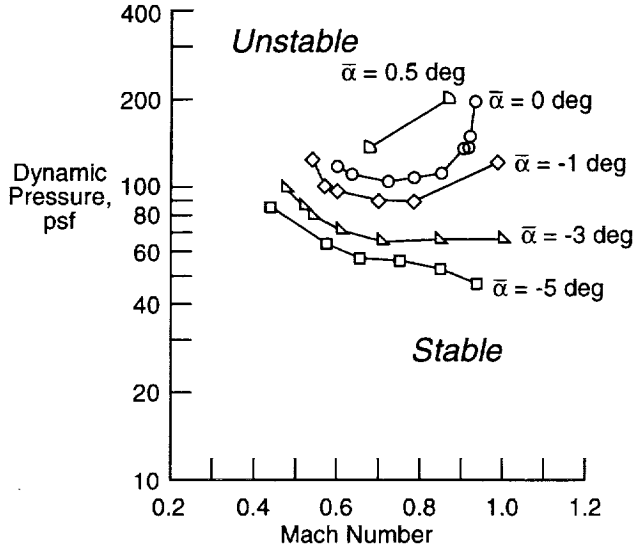

Fig. 43 Experimental flutter boundaries for the HSR-RSM model on the PAPA mount.

simple table of measured structural properties is not presented here. These parameters are available as part of the RSM experimental data set. Additionally, reference 57 describes the ground vibration tests that were performed on the RSM/PAPA. For the various configurations, this report includes measured frequencies, mode shapes, and damping for the primary vibratory modes, pitch and plunge.

Two finite element models were developed for the FSM. These finite element representations were independently correlated to static-load deflection data and Ground Vibration Test data of the model and mount. One of the FEMs was constructed for use with MSC/NASTRAN. The other FEM was constructed using the ELFINI analysis system. The MSC/NASTRAN FEMs are discussed in references 58 and 59, and are available for distribution along with the wind-tunnel data sets.

Aerodynamic Models and Analyses

As part of the HSR program a variety of computational analyses were performed for the RSM and FSM configurations. Much of this work was published as contractor reports under NASA contract NAS1-20220, and while not generally available, these HSR reports can be obtained from the NASA Langley Research Center Technical Library.

For the RSM model mounted to the balance, steady and unsteady analysis test correlation studies were performed by The Boeing Company. References 60, 61, and 62 document the steady and unsteady (flap dwell) correlation studies. The codes used in these studies were MSC/NASTRAN, ZONA, PANAIR (A502), TRANAIR, and CFL3D.[63] The TRANAIR and CFL3D codes were used in both inviscid and viscous modes to study the effects of a viscous boundary layer.

References 64, 65, and 58 summarize the analysis test correlation studies that were performed for the FSM. The studies that are documented in these reports can be categorized into two general types, static aeroelastic and dynamic aeroelastic. For the static aerolastic cases four code combinations were explored: 1) ELFINI with PANAIR aerodynamics, 2) ELFINI with TRANAIR aerodynamics, 3) MSC/NASTRAN with doublet lattice aerodynamics, and 4) MSC/NASTRAN with CFL3D.AE-BA[66] aerodynamics. Three code combinations were also explored for the dynamic aerolastic case. They were 1) MSC/NASTRAN with doublet lattice aerodynamics, 2) MSC/NASTRAN with CFL3D.AE-BA, and 3) ELFINI with ELFINI SINGULARITY doublet lattice aerodynamics.

To date, correlation of analysis with experimental FSM flutter data has been one of the most challenging aspects of these studies. The linear FSM flutter analyses were performed pre- and post-wind-tunnel test. These analyses indicated that two flutter mechanisms were present. The first mechanism is referred to as a "hump" mode. Hump modes exhibit great sensitivity to damping and are usually difficult to predict accurately. The second mechanism is referred to as a "hard" flutter mechanism, a coalescence of the third and fourth modes. Figure 42 contains a pre-test linear analytical prediction of the flutter boundary. The pre-test analytical boundary was traversed several times during the flutter test without a flutter incident, in-

dicating a discrepancy in the aeroelastic model. An updated linear flutter boundary was obtained using an optimized FEM[59] and is presented and discussed in reference 58. The updated linear flutter boundary has a flutter dynamic pressure slightly above the hard flutter point and, therefore, appears to be an improvement of the pre-test linear flutter prediction. In spite of this improvement, these linear analyses failed to capture the chimney flutter boundary. Reference 58 describes the nonlinear aeroelastic analyses performed for the FSM configuration using the MSC/NASTRAN with CFL3D.AE-BA code combination. In this study, CFL3D was run in the inviscid mode and succeeded in capturing the chimney phenomenon shown in figure 42.

MAVRIC-I Business Jet Wing

LaRC's Aeroelasticity Branch is actively developing analytical methods and associated validation experiments to investigate unsteady flows, particularly those that exhibit strong flow nonlinearities. As part of this effort, a program known as Models for Aeroelastic Validation Research Involving Computations (MAVRIC) is being developed and implemented to provide experimental data for use in high-level aeroelastic code validation. An existing aeroelastically scaled model of a business jet wing has been modified to measure unsteady surface pressures and has recently been tested in the TDT.

This model was chosen for testing based upon its simple construction, simple finite element structural modeling, and its aeroelastic behavior in the 0.80 to 0.90 Mach number range. Previous TDT tests at these conditions showed that model motions were predominantly in the first wing-bending mode and exhibited a characteristic response termed Limit Cycle Oscillation (LCO). Here wing motions are seen to have a generally periodic response whose average amplitude is rather constant for constant tunnel conditions, and which increases in amplitude for small increases in tunnel conditions (Mach number, dynamic pressure, and sometimes angle of attack). Instances of LCO behavior are of great interest to aeroelasticians and are encountered under conditions of high-speed separation onset. They involve strong shock-boundary layer interaction and have been very difficult to study experimentally or computationally.

Physical Description

This model was originally constructed as a simple plate flutter model of a business jet wing mounted low on a fuselage body of revolution. Figure 44 shows the model mounted to the tunnel sidewall. The stepped aluminum plate providing the wing stiffness was fitted with end-grain balsa wood to provide the wing contour. The wing has a taper ratio of 0.29 and a mid-chord sweep of 23 degrees. The wing thickness

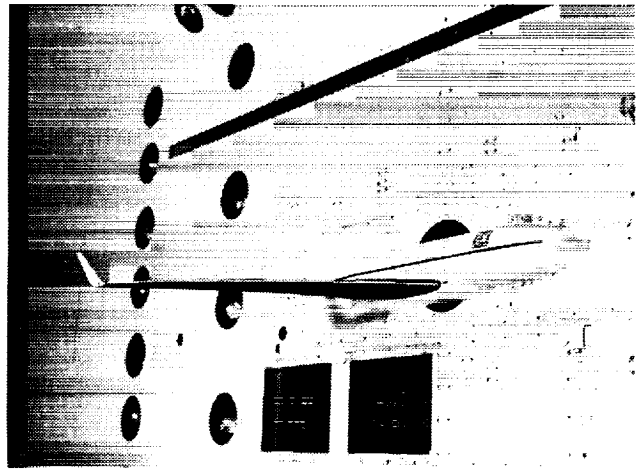

Fig. 44 Original business jet wing model mounted in TDT test section.

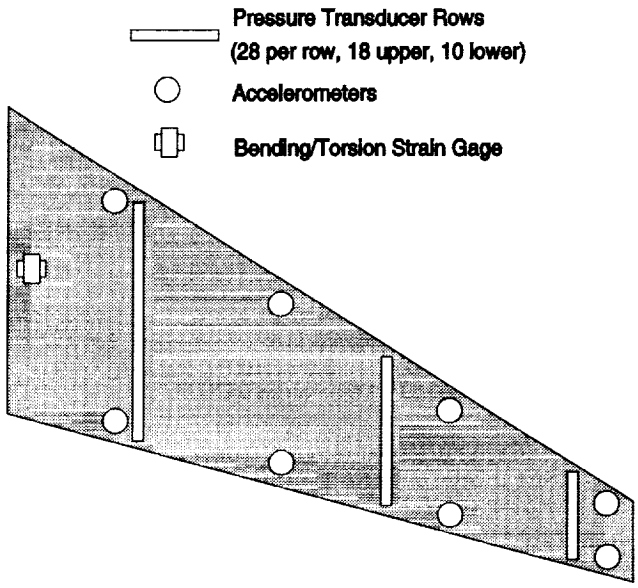

Fig. 45 Instrumentation layout for refurbished MAVRIC-I business jet wing model.

varies from 13 percent chord at the symmetry plane to 8.5 percent chord at the wing tip. The first eight wind-off modal frequencies of the model range from 4 Hz. to 75 Hz.

Figure 45 indicates the location of the unsteady pressure instrumentation that has been added to the model. Three chords of unsteady pressure transducers are installed at nondimensional span stations 0.22, 0.63, and 0.87. Each chord has 18 upper surface and 10 lower surface close-mounted transducers. Eight accelerometers are mounted along the leading and trailing edge of the wing, and a bending/torsion strain gage was installed at the root.

Experimental Data Set

The model was originally tested with three wingtip configurations: cutoff wingtip, winglet, and tip "pencil" store body of revolution. Flutter boundaries were

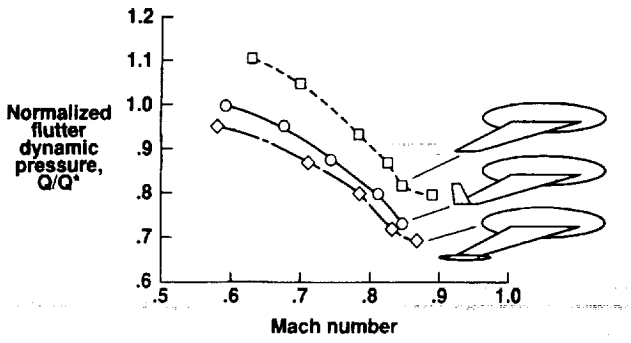

Fig. 46 Measured business jet wing flutter boundary with three wing tip configurations.

measured in air and in heavy gas for most of the combinations of wing tip configuration and gas. Figure 46 shows flutter boundaries measured in air for the three tip configurations with the flutter dynamic pressure normalized by its value at M = 0.6 for the "nominal" winglet configuration. The intent of the retest is to obtain unsteady pressure and wing response data under conditions of transonic buffeting, separation onset, and LCO in order to validate CFD codes for such conditions.

Structural Model

The structural model of the MAVRIC-I wind-tunnel model consists of an MSC/NASTRAN finite element model. The FEM was constructed using plate elements to represent the aluminum plate and solid elements to represent the end-grain balsa. The original version of this FEM was used to generate the generalized mass, stiffness, and mode shapes for the study described in reference 67. This FEM has been updated to include recent modifications to the wind-tunnel model. The MAVRIC-I FEM is available for distribution along with the experimental data.

Aerodynamic Models and Analyses

Edwards[68] has published calculations of the LCO behavior of the cutoff wingtip for the M = 0.89 case using an interactive boundary layer model. Figure 47 shows the computed transient time history of the wingtip responses for large and small initial wing displacements. The characteristics of the LCO behavior are seen, with the response growing to the limit cycle amplitude for the smaller initial condition and decaying to the limit cycle amplitude for the larger initial value.

In addition to the LCO calculations discussed above, Gibbons[67] performed extensive flutter computations for the cutoff wingtip version of this model. Both viscous and inviscid calculations were performed demonstrating the striking role viscosity can play in predicting the flutter boundary for this wing. These results are summarized in figure 48. The top figure plots the flutter speed index as a function of Mach number while

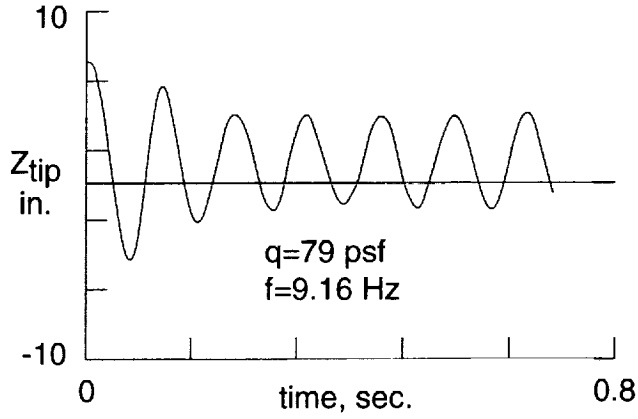

a) Amplitude decaying to limit cycle oscillation.

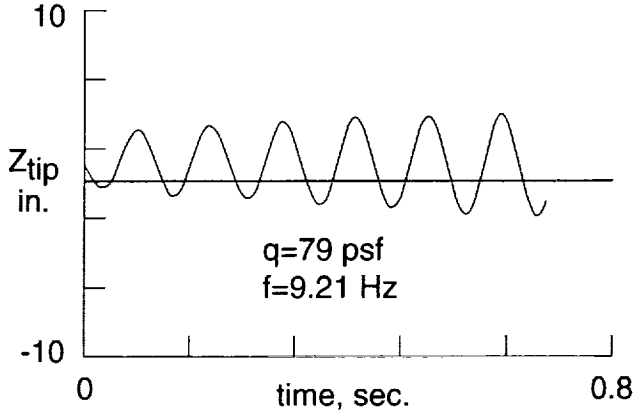

b) Amplitude growing to limit cycle oscillation.

Fig. 47 Business jet computed wing tip deflection time histories showing limit cycle oscillation, M = 0.89.

the bottom figure displays the flutter frequency as a function of Mach number. An aeroelastic version of CFL3D was used for these computations which shows the flutter velocity and frequency rapidly decreasing in the transonic range for the inviscid Euler computations. Similar results were obtained using the inviscid transonic small disturbance potential flow equations. The addition of viscosity to the computations corrects this rapid decrease and predicts a flutter boundary that is closer to the measured boundary and more representative of the classical transonic dip seen on this class of wing. The modifications to this model to include the measurement of unsteady pressures have provided more detailed data that can be used to analyze and interpret both viscous and inviscid computations and better understand the role of viscosity in flutter calculations.

Oscillating Turntable

A forced-oscillation device capable of pitching large-scale models at relatively high frequencies would be a valuable tool for generating computational code validation data and general research in the area of

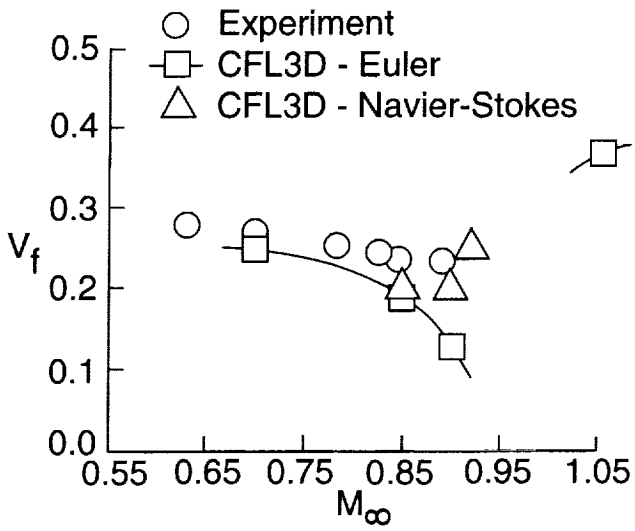

a) Flutter speed index.

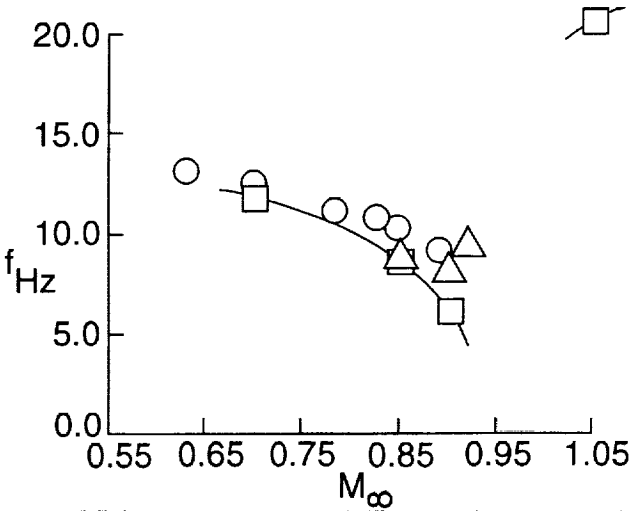

b) Flutter frequency.

Fig. 48 Flutter computations for the clean wing version of the MAVRIC-I model.

unsteady aerodynamics. To this end, an oscillating turntable (OTT) mechanism has been developed, installed, and tested in the TDT. This device is shown in figure 49. The OTT is mounted on a platform that is cantilevered off the east wall of the TDT. The OTT sits on a pair of floor rails that allow it to be retracted away from the TDT wall for ease of maintenance and access to the tunnel wall. In the figure, the OTT is in the retracted position. Models are mounted to the end of the pitch strut after the unit has been moved to its forward position. The turntable consists of a rotary hydraulic actuator and support equipment capable of generating 495,000 in-lbs of torque, a bearing housing for the pitch strut, and a disk brake mechanism for stopping model oscillations. The unit is designed to sinusoidally oscillate models about mean angles-of-

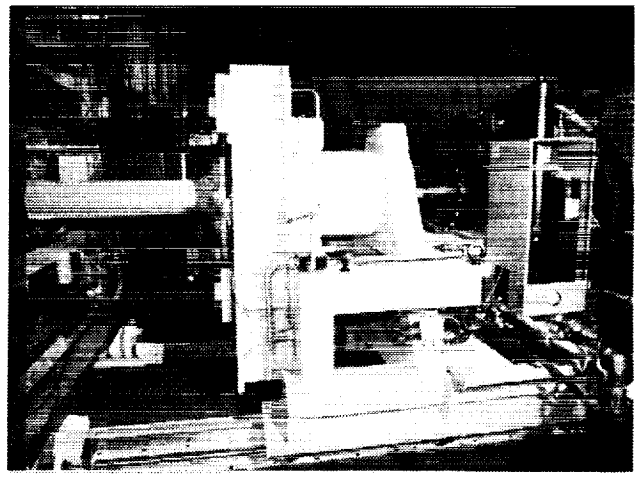

Fig. 49 TDT Oscillating Turntable (OTT).

attack between -15 and +45 degrees with pitch inertias as large as 65,000 lbm-in^2 at frequencies up to 40 Hz and 1 degree pitch amplitude. Models with pitch inertias up to 250,000 lbm-in^2 can be oscillated at up to 20 Hz and 1 degree amplitude. The OTT is also capable of oscillating both of these models at 1 Hz and up to 10 degrees amplitude. Given these capabilities and the power required to meet them, numerous fail-safe, emergency shutdown, and safety features have been designed into the OTT. At the heart of this system is a disk brake capable of stopping the model within 15 degrees of motion after the brake is applied. In addition to fail-safe systems that activate the brake in an emergency stop situation or when electrical and/or hydraulic power are lost, the hydraulic actuator also jogs to a low-power mode whenever the TDT test section access door is open.

The OTT and its support systems have been installed in the TDT. The OTT has been tested in a wind-off mode in the tunnel and its performance specifications have been verified. Wind-on testing with the OTT is scheduled for summer 2000 using the HSR-RSM and BSCW, previously described in this paper, as the test articles. A second entry to test a large commercial transport model is scheduled for early 2001.

Concluding Remarks

NASA LaRC researchers have been involved in the measurement of unsteady pressures for nearly 40 years. For the past 20 years, these measurements have focused on providing detailed unsteady aerodynamics data for use in CFD code development, evaluation, and validation. Cases ranging in geometric complexity from a simple two-dimensional rigid airfoil to a complex, structurally flexible wing/fuselage configuration have been highlighted in this paper. Likewise the flow conditions covered by these cases range from attached subcritical flow to highly nonlinear flows involving shock waves, boundary layer separation, vortices and combinations of these phenomena. Often the appear-

ance of these phenomena is transient, making some of these conditions quite challenging for computational methods. Several of the datasets presented in this paper were acquired more than 20 years ago and have not been highly utilized since their acquisition. However, their age should not be a factor that discounts their usefulness for code validation.

The complexity and resource requirements for unsteady computations have significantly stunted the development of CFD methods for these types of problems. Therefore, these datasets have been somewhat ahead of their time in that they existed well before methods that could effectively predict them were available. As computer hardware, numerical algorithms, and computational techniques have progressed, these data have begun to enjoy more attention as evidenced by the computations presented and referenced in this paper. It is expected that this attention will continue to increase with the publication of the NATO Research and Technology Organization (RTO) working group document on experimental and computational test cases for computational method validation.[18]

LaRC researchers continue to identify unsteady aerodynamic and aeroelastic phenomena relevant to modern aircraft design and formulate experiments and experimental techniques to investigate these problems. Current and future research activities involving unsteady pressure measurements will focus on highly nonlinear phenomena, such as Limit Cycle Oscillation (LCO), which involve shock-boundary layer interaction, separated flows and structural interactions. Model construction approaches, instrumentation, test techniques, and data acquisition systems continue to evolve, and LaRC researchers are exploiting these developments to formulate new and innovative methods to efficiently and accurately acquire unsteady pressure data. These capabilities will allow researchers to further explore relevant unsteady flow phenomena and continue to provide high-quality, detailed aerodynamics data for computational aerodynamics, aeroelasticity and controls research.

Requesting Data Sets

To receive data sets, a written request must be sent to:

Aeroelasticity Branch
Mail Stop 340
NASA Langley Research Center
Hampton, VA 23681

References

[1]Schuster, D. M., Edwards, J. W., and Bennett, R. M., "An Overview of Unsteady Pressure Measurements in the Transonic Dynamics Tunnel," *AIAA Dynamics Specialists Conference*, No. 2000-1770, Atlanta, GA, April 2000.

[2]Cole, S. R. and Garcia, J. L., "Past Present and Future Capabilities of the Transonic Dynamics Tunnel from an Aeroelasticity Perspective," *AIAA Dynamics Specialists Conference*, No. 2000-1767, Atlanta, GA, April 2000.

[3]Rivera, Jr., J. A. and Florance, J. R., "Contributions of Transonic Dynamics Tunnel Testing to Airplane Flutter Clearance," *AIAA Dynamics Specialists Conference*, No. 2000-1768, Atlanta, GA, April 2000.

[4]Cole, S. R., Keller, D. F., and Piatak, D. J., "Contributions of Transonic Dynamics Tunnel to Launch Vehicle and Spacecraft Development," *AIAA Dynamics Specialists Conference*, No. 2000-1772, Atlanta, GA, April 2000.

[5]Perry, III, B., Noll, T. E., and Scott, R. C., "Contributions of Transonic Dynamics Tunnel Testing of Active Control of Aeroelastic Response," *AIAA Dynamics Specialists Conference*, No. 2000-1769, Atlanta, GA, April 2000.

[6]Yeager, Jr., W. T. and Kvaternik, R. G., "Contributions of Langley Transonic Dynamics Tunnel to Rotorcraft Technology and Development," *AIAA Dynamics Specialists Conference*, No. 2000-1771, Atlanta, GA, April 2000.

[7]Hess, R. W., Seidel, D. A., Igoe, W. B., and Lawing, P. L., "Transonic Unsteady Pressure Measurements on a Supercritical Airfoil at High Reynold Number," *Journal of Aircraft*, Vol. 26, No. 7, July 1989, pp. 605–614.

[8]Bartels, R. E. and Edwards, J. W., "Cryogenic Tunnel Pressure Measurements on a Supercritical Airfoil for Several Shock Buffet Conditions," NASA TM 110272, Sept. 1997.

[9]Ng, W. F. and Rosson, J. C., "Cryogenic Tunnel Measurement of Total Temperature and Pressure," *Journal of Aircraft*, Vol. 23, No. 3, March 1986, pp. 244–249.

[10]Bartels, R. E., "Computation of Shock Buffet Onset for a Conventional and Supercritical Airfoil," AIAA 97–0833, Jan. 1997.

[11]Bartels, R. E., "Flow and Turbulence Modeling and Computation of Shock Buffet Onset for Conventional and Supercritical Airfoils," NASA TP 1998-206908, Feb. 1998.

[12]McDevitt, J. B. and Okuno, A. F., "Static and Dynamic Pressure Measurements on a NACA 0012 Airfoil in the Ames High Reynolds Number Facility," NASA TP 2485, 1985.

[13]Edwards, J. W., "Transonic Shock Oscillations Calculated with a New Interactive Boundary Layer Coupling Method," AIAA 93–0777, 1993.

[14]Ricketts, R. H., Sandford, M. C., Seidel, D. A., and Watson, J. J., "Transonic Pressure Distributions on a Rectangular Supercritical Wing Oscillated in Pitch," *Journal of Aircraft*, Vol. 21, No. 8, Aug. 1984, pp. 576–582.

[15]Ricketts, R. H., Sandford, M. C., Watson, J. J., and Seidel, D. A., "Subsonic and Transonic Unsteady-and Steady-Pressure Measurements on a REctangular Supercritical Wing Oscillated in Pitch," NASA TM 85765, Aug. 1984.

[16]Ricketts, R. H., Sandford, M. C., Watson, J. J., and Seidel, D. A., "Geometric and Structural Properties of a Rectangular Supercritical Wing Oscillated in Pitch for Measurements of Unsteady Transonic Pressure Distributions," NASA TM 85673, Nov. 1983.

[17]Bennett, R. M. and Walker, C. E., "Computational Test Cases for a Rectangular Supercritical Wing Undergoing Pitching Oscillations," NASA TM 1999-209130, April 1999.

[18]"Verification and Validation Data for Computational Unsteady Aerodyanmics Codes," No. 26, Applied Vehicles Technology Working Group-003 of the NATO Research and Technology Organization, 2000.

[19]Whitcomb, R. T., "Review of NASA Supercritical Airfoils," ICAS Paper 74-10, Aug. 1974.

[20]Hess, R. W., Cazier, Jr., F. W., and Wynne, E. C., "Steady and Unsteady Transonic Pressure Measurements on a Clipped Delta Wing for Pitching and Control-Surface Oscillations," NASA TP 2594, Oct. 1986.

[21]Hess, R. W., Cazier, Jr., F. W., and Wynne, E. C., "Static and Unsteady Pressure Measurements on a 50 degree Clipped Delta Wing at M = 0.9," AIAA 82-0686, 1982.

[22]Bennett, R. M. and Walker, C. E., "Computational Test Cases For a Clipped Delta Wing with Pitching and Trailing-Edge Control Surface Oscillation," NASA TM 1999-209104, March 1999.

[23]Bhatia, K. G. and Wertheimer, J., "Aeroelastic Challenges for a High Speed Civil Transport," AIAA 93-1478, May 1993.

[24]Bennett, R. M., Eckstrom, C. V., Rivera, J. A., Dansberry, B. E., Farmer, M. G., and Durham, M. H., "The Benchmark Aeroelastic Models Program - Description and Highlights of Initial Results," AGARD CP 507, March 1992.

[25]Rivera, Jr., J. A., Dansberry, B. E., Durham, M. H., Bennett, R. M., and Silva, W. A., "Pressure Measurements on a Rectangular Wing with A NACA 0012 Airfoil During Conventional Flutter," NASA TM 104211, July 1992.

[26]Rivera, Jr., J. A., Dansberry, B. E., Bennett, R. M., Durham, M. H., and Silva, W. A., "NACA 0012 Benchmark Model Experimental Flutter Results With Unsteady Pressure Distributions," NASA TM 107581, March 1992.

[27]Rivera, Jr., J. A., Dansberry, B. E., Farmer, M. G., Eckstrom, C. V., Seidel, D. A., and Bennett, R. M., "Experimental Flutter Boundaries with Unsteady Pressure Distributions for the NACA 0012 Benchmark Model," AIAA 91-1010, 1991.

[28]Rivera, Jr., J. A., Dansberry, B. E., Bennett, R. M., Durham, M. H., and Silva, W. A., "NACA 0012 Benchmark Model Experimental Flutter Results With Unsteady Pressure Distributions," AIAA 92-2396, April 1992.

[29]Dansberry, B. E., Durham, M. H., Bennett, R. M., Rivera, Jr., J. A., Silva, W. A., and Wieseman, C. D., "Experimental Unsteady Pressures at Flutter on the Supercritical Wing Benchmark Model," AIAA 93-1592, April 1993.

[30]Dansberry, B. E., Durham, M. H., Bennett, R. M., Turnock, D. L., Silva, W. A., and Rivera, Jr., J. A., "Physical Properties of the Benchmark Models Program Supercritical Wing," NASA TM 4457, Sept. 1993.

[31]Dansberry, B. E., "Dynamic Characteristics of a Benchmark Models Program Supercritical Wing," AIAA 92-2368, April 1992.

[32]Farmer, M. G., "A Two-Degree-of-Freedom Flutter Mount System with Low Damping for Testing Rigid Wings at Different Angles of Attack," NASA TM 83302, 1982.

[33]Farmer, M. G., "Mount System for Testing Flutter," Oct. 1984, U.S. Patent 4,475,385.

[34]Durham, M. H., Keller, D. F., Bennett, R. M., and Wieseman, C. D., "A Status Report on a Model for Benchmark Active Controls Testing," AIAA 91-1011, April 1991.

[35]Scott, R. C., Hoadley, S. T., Wieseman, C. D., and Durham, M. H., "The Benchmark Active Controls Technology Model Aerodynamic Data," *Proceedings of the 35th Aerospace Sciences Meeting and Exhibit*, No. 97-0829, Reno, NV, Jan. 1997.

[36]Waszak, M. R., "Modeling the Benchmark Active Control Technology Wind-Tunnel Model for Application to Flutter Suppression," AIAA 96-3437, July 1996.

[37]Waszak, M. R., "BACT Simulation User Guide," NASA TM 97-206252, Nov. 1997.

[38]Peele, E. L. and Adams, W. M., "A Digital Program for Calculating the Interaction Between Flexible Structures, Unsteady Aerodynamics, and Active Controls," NASA TM 80040, Jan. 1979.

[39]Bartels, R. E. and Schuster, D. M., "Comparison of Two Navier-Stokes Aeroelastic Methods Using BACT Benchmark Experimental Data," *17th Applied Aerodynamics Conference*, No. 99-3157, Norfolk, VA, June 1999, pp. 433-443.

[40]Murrow, H. N. and Eckstrom, C. V., "Drones for Aerodynamic and Structural Testing (DAST)-A Status Report," *Journal of Aircraft*, Vol. 16, Aug. 1979, pp. 521-526.

[41]Sandford, M. C., Seidel, D. A., Eckstrom, C. V., and Spain, C. V., "Geometrical and Structural Properites of an Aeroelastic Research Wing (ARW-2)," NASA TM 4110, April 1989.

[42]Seidel, D. A., Sandford, M. C., and Eckstrom, C. V., "Measured Unsteady Transonic Aerodynamics Characteristics of an Elastic Supercritical Wing," *Journal of Aircraft*, Vol. 24, No. 4, April 1987, pp. 225-230.

[43]Sandford, M. C., Seidel, D. A., and Eckstrom, C. V., "Steady Pressure Measurements on an Aeroelastic Research Wing (ARW-2)," NASA TM 109046, Feb. 1994.

[44]Byrdsong, T. A., Adams, R. R., and Sandford, M. C., "Close-Range Photogrammetric Measurements of Static Deflections for an Elastic Supercritical Wing," NASA TM 4194, Dec. 1990.

[45]Seidel, D. A., Sandford, M. C., and Eckstrom, C. V., "Unsteady-Pressure and Dynamic-Deflection Measurements on an Aeroelastic Supercritical WIng," NASA TM 4278, Dec. 1991.

[46]Seidel, D. A., Eckstrom, C. V., and Sandford, M. C., "Transonic Region of High Dynamic Response Encountered on an Elastic Supercritical Wing," *Journal of Aircraft*, Vol. 26, No. 9, Sept. 1989, pp. 870-875.

[47]Eckstrom, C. V., Seidel, D. A., and Sandford, M. C., "Unsteady Pressure and Structural Response Measurements on an Elastic Supercritical Wing," *Journal of Aircraft*, Vol. 76, No. 1, Jan. 1990, pp. 75-80.

[48]Eckstrom, C. V., Seidel, D. A., and Sandford, M. C., "Measurements of Unsteady Pressure and Structural Response for an Elastic Supercritical Wing," NASA TP 3443, Nov. 1994.

[49]Moses, G. F. and Pierce, D., "The Dynamics Response of Wings in Torsion at High Subsonic Speed," AGARD CP 226, April 1977.

[50]Engineering Information Systems, Inc., *EISI-SPAR Reference Manual - System Level 103*, Jan. 1979.

[51]Engineering Information Systems, Inc., *EISI-EAL Engineering Analysis Language Reference Manual*, 1983.

[52]Spain, C. V., "Development of a NASTRAN Finite Element of the Aeroelastic Research Wing (ARW-2)," LMES ASR 99-05, Oct. 1999.

[53]Farhangnia, M., Guruswamy, G., and Biringen, S., "Transonic-Buffet Associated Aeroelasticity of a Supercritical Wing," *34th Aerospace Sciences Meeting and Exhibit*, No. 96-0286, Jan. 1996.

[54]Silva, W. A., Keller, D. F., Florance, J. R., Cole, S. R., and Scott, R. C., "Experimental Steady and Unsteady Aerodynamic and Flutter Results for HSCT Semispan Models," *Proceedings of the 41st AIAA/ASME/ASCE/AHS/ASC Structures, Structural Dynamics, and Materials Conference*, No. 2000-1697, Atlanta, GA, April 2000.

[55]Schuster, D. M. and Rausch, R. D., "Transonic Dynamics Tunnel Force and Pressure Data Acquired on the HSR Rigid Semispan Model," NASA CR 199-209555, Sept. 1999.

[56]Schuster, D. M., Spain, C. V., Turnock, D. L., Rausch, R. D., Hamouda, M.-N., Vogler, W. A., and Stockwell, A. E., "Development, Analysis, and Testing of the High Speed Research Flexible Semispan Model," NASA CR 199-209556, Sept. 1999.

[57]Spain, C. V. and Javeed, M., "Vibration Testing of the HSR Rigid Semi-span Model Mounted on the Pitch and Plunge Apparatus," LMES ASR 98-03, Oct. 1998.

[58]Baker, M. L., Mendoza, R., and Hartwich, P. M., "Transonic Aeroelastic Analysis of a High Speed Transport Wind Tunnel Model," *Proceedings of the 40th AIAA/ASME/ASCE/AHS/ASC Structures, Structural Dynamics, and Materials Conference*, No. 99-1217, St. Louis, MO, April 1999.

[59]Bartkowicz, T. J., Kim, H. M., and Kaouk, M., "Model Correlation of the Flexible Semispan Model," *18th International Modal Analysis Conference*, San Antonio, TX, Feb. 2000.

[60]"Rigid Semispan Model (RSM) Analysis-Test Correlation," Tech. Rep. CRAD-9408-TR-2433, Oct. 1996.

[61]"Correlation of A502 (PANAIR) and TRANAIR Inviscid Results with NASA Langley TDT Test 520 Data for the HSR Rigid Semi-Span Model," Tech. Rep. DTF26-2-01, March 1997.

[62] "Rigid Semispan Model (RSM) with Flap Analysis-Test Correlation," Tech. Rep. CRAD-9408-TR-3691-2-01, Sept. 1997.

[63] Thomas, J. L., Krist, S. L., and Anderson, W. K., "Navier-Stokes Computation of Vortical Flows Over Low Aspect Ratio Wings," *AIAA Journal*, Vol. 28, 1990, pp. 205-212.

[64] "Flexible Semispan Model (FSM) Analysis-Test Correlation," Tech. Rep. CRAD-9408-TR-3342, Sept. 1997.

[65] "Analysis-Test Correlation of the HSR Flexible Semispan Model," Tech. Rep. DTF26-2-02, Nov. 1997.

[66] Hartwich, P. M. and Agrawal, S., "Method for Perturbing Multiblock Patched Grids in Aeroelastic and Design Optimization Applications," *AIAA Applied Aerodynamics Conference*, No. 97-2038, June 1997.

[67] Gibbons, M. D., "Aeroelastic Calculations Using CFD for a Typical Business Jet Model," NASA Contractor Report 4753, Sept. 1996.

[68] Edwards, J. W., "Calculated Viscous and Scale Effects on Transonic Aeroelasticity," AGARD R-822, March 1998.